Published in final edited form as:
Adv Drug Deliv Rev. 2013 July ; 65(8): 1098–1111. doi:10.1016/j.addr.2012.10.012.

Mapping Biological Behaviors by Application of Longer-Lived Positron Emitting Radionuclides

Yang Zhou, **Kwamena E. Baidoo**, and **Martin W. Brechbiel***
Radioimmune & Inorganic Chemistry Section, ROB, NCI, NIH, Bethesda, Maryland, USA

Abstract

With the technological development of positron emission tomography (PET) and the advent of novel antibody-directed drug delivery systems, longer-lived positron-emitting radionuclides are moving to the forefront to take important roles in tracking the distribution of biotherapeutics such as antibodies, and for monitoring biological processes and responses. Longer half-life radionuclides possess advantages of convenient on-site preparation procedures for both clinical and non-clinical applications. The suitability of the long half-life radionuclides for imaging intact monoclonal antibodies (mAbs) and their respective fragments, which have inherently long biological half-lives, has attracted increased interest in recent years. In this review, we provide a survey of the recent literature as it applies to the development of nine-selected longer-lived positron emitters with half-lives of 9–140 hours (e.g., ^{124}I, ^{64}Cu, ^{86}Y and ^{89}Zr), and describe the biological behaviors of radionuclide-labeled mAbs with respect to distribution and targeting characteristics, potential toxicities, biological applications, and clinical translation potentials.

Keywords

immuno-PET; radioimmunoimaging; monoclonal antibodies; oncology; ^{86}Y; ^{89}Zr; ^{124}I; ^{64}Cu

1. Introduction

Positron emission tomography (PET) employs a radionuclide, incorporated into a molecule, to non-invasively study specific biological processes both quantitatively and qualitatively in real-time mode. Unlike computed tomography (CT) and magnetic resonance imaging (MRI), PET can detect the initial molecular changes in response to treatment before anatomical alteration. Therefore, PET has the potential to evaluate the effectiveness of a treatment plan at earlier time points [1,2] and to assess the efficacy of new drugs preclinically and clinically. When integrated with CT or MRI, PET can be more accurate due to the anatomical and molecular co-registration from integration of these imaging modalities. Moreover, PET has superiority over single-photon emission computed tomography (SPECT) in terms of sensitivity, spatial resolution, and quantitation of radioactivity in tissues. Currently, PET, as a powerful molecular technology, is playing an increasingly important role in the diagnosis, staging, restaging, and monitoring response to treatment of cancers in clinical settings. In addition, PET has been applied to identify the biological characteristics of cancer (molecular events, pharmacokinetics, etc.), providing valuable information for new drug development. There are at this time 552 PET-involved

*To whom correspondence should be addressed: Martin W. Brechbiel, Radioimmune & Inorganic Chemistry Section, Radiation Oncology Branch, NCI, NIH, 10 Center Drive, Building 10, Rm B3B69, Bethesda, Maryland 20892-1002, USA. Phone: 301-496-0591; Fax 301-402-1923; martinwb@mail.nih.gov..

ongoing oncology clinical trials that further demonstrate the promise of PET (data from http://clinicaltrials.gov).

Currently, ^{18}F-FDG (2-[^{18}F] fluoro-2-deoxy-D-glucose) is the only agent approved by the U.S. Food and Drug Administration (FDA) for clinical PET imaging in oncology. This agent is used as a glucose metabolic marker to measure the malignant activity on the basis of increased glucose uptake and metabolism in cancer cells. From clinical data, the average sensitivity and specificity of ^{18}F-FDG are 84% and 88%, respectively [3]. ^{18}F-FDG is now frequently employed as a standard when a new PET radiotracer is in development for clinical use. Indeed, the broad use of ^{18}F-FDG in oncology in turn boosts the development of new PET radiotracers.

With the ongoing advances in biotherapeutics and antibody-directed drug delivery systems, it becomes important to be able to screen patients prior to specific antibody therapies, and to design personalized therapeutic regimens, thereby avoiding unnecessary toxicities. Currently, 30 therapeutic monoclonal antibodies (mAbs) have been approved by the FDA [4]; however, only a few radiolabeled mAbs have gained approval for use in clinical oncology, including four immunodiagnostic agents and two radioimmunotherapeutic agents [5]. Immuno-PET, which refers to PET studies that employ radiolabeled mAbs or their respective fragments as vehicles for specific delivery of β^+-emitting radionuclides, is one of the most promising fields in clinical oncology. This paradigm is believed to provide greater disease specificity as compared to FDG-PET, which is actually a metabolic marker, and to provide phenotypic information on tumor-associated antigen/receptor expression that can guide the management of the therapy of primary and metastatic lesions. For the purpose of labeling antibodies and their fragments, the half-life of ^{18}F ($t_{1/2}$ = 1.8 h) is too short to fulfill the requirements for long-duration PET studies that require longer half-life β^+-emitters. It cannot be neglected that continuing efforts are being made to further improve and broaden the application of the commonly used “standard PET radionuclides”, ^{18}F, ^{11}C ($t_{1/2}$ = 20 min), ^{13}N ($t_{1/2}$ = 10 min), ^{15}O ($t_{1/2}$ = 2 min). For example, a simple ^{18}F-labeling method, developed by McBride et al. [6], was successfully applied to label a NOTA-conjugated BBN analog and image prostate tumors [7]. However, the short half-life of ^{18}F limits the vector molecules to pharmacokinetically-matched small molecules or peptides, rather than proteins that stay *in vivo* for as long as 1–3 weeks [8].

Longer half-life radionuclides possess advantages suitable for convenient on-site preparation procedures even in the clinic. In recent years, increased interest in these radionuclides has arisen from the need to image the inherently long biological half-lives of intact mAbs and their respective fragments in vivo. Adequate imaging of the distribution of these biologicals requires complementary long half-life radionuclides to allow studies of long duration. A comprehensive description of longer-lived β^+-emitters, with respect to radiochemistry, is provided elsewhere [9]. However, to be an ideally effective clinical immuno-PET probe for cancer studies, numerous criteria need to be fulfilled (Table 1). Although it is irresoluble to satisfy all the requirements, all factors should be considered and weighed when a probe is designed for immuno-PET imaging. In this review, we provide a survey of the recent literature as it applies to the development of nine-selected long-lived β^+-emitters with half-lives of 9–140 hours (e.g. ^{124}I, ^{64}Cu, ^{86}Y and ^{89}Zr) (Table 2). We describe the biological behaviors of radionuclide-labeled mAbs with respect to distribution and targeting characteristics, potential toxicities, biological applications, and clinical translation potentials. This review also highlights recently reported preclinical and clinical applications of immuno-PET. The PET nuclides are arranged in order of increasing atomic mass.

2. Longer-lived positron emitting radionuclides

Tumor delivery and distribution of mAbs can be evaluated by PET using radiolabeled mAbs. Only relatively recently have technical advances in the production of longer-lived β^+-emitters allowed immuno-PET research to move forward in preclinical and clinical applications. When predicting the biodistribution of a complementary radioimmunotherapy (RIT) agent and determining dosing by an antibody-based PET probe, the characteristics of biodistribution in healthy subjects, as well as animal models, facilitate the understanding and explanation of the imaging data in patients. Given that an immuno-PET agent is mainly composed of an antibody (or its fragment) and a corresponding radionuclide, it is instructive to compare the radiotracers with the same antibody labeled by different radionuclides to elucidate the differences between emitters. Valuable information on an emitter can also be provided by labeling different antibodies with the same radionuclide. An example is the comparison of ^{76}Br- and ^{125}I- labeled anti-carcinoembryonic antigen (CEA) mAb 38S1 in PET imaging [10]. The differences observed in distribution, organ uptake, pharmacokinetics and catabolism can be mainly attributed to distinct radionuclides.

The targets of antibodies for immuno-PET include the antigens present on tumor cells (e.g. prostate-specific membrane antigen (PSMA), epidermal growth factor receptor (EGFR/HER-2), epithelial cell adhesion molecule (EpCAM)) and tumor vasculatures (e.g. vascular endothelial growth factor (VEGF), integrin) (Fig. 1). Cell surface proteins in the target tissue are especially attractive because they are readily accessible to extracellular mAbs or peptide probes. VEGF is a different example. After production in tumor cells under hypoxia, VEGF is secreted into the extracellular matrix (ECM), and then binds to its receptors on endothelial cells leading to initiation of angiogenesis. Accordingly, VEGF is distributed intracellularly, in the ECM, and on endothelial cells. However, remarkably, ^{89}Zr-bevacizumab was suggested as binding to VEGF primarily within the blood vessels of the tumor [11].

Mapping of the antigen expression by immuno-PET is beneficial for individual treatment decisions and helps obtain effective personalized therapeutic response to antibody or other therapeutic drugs. This is especially important due to the characteristics of heterogeneity of tumors. High inter-and intra-tumoral heterogeneity of cancer biomarkers has been frequently observed in PET studies [12–14]. Furthermore, whole-body distribution patterns, as well as antibody clearance rate of the same radiotracer, can also vary from one person to another due to inter-individual variations [12].

Additionally, the biodistribution characteristics of radiopharmaceuticals provide valuable information on the potential toxicities of new mAbs and drugs along with dosimetric data for RIT planning; multiple longitudinal scans of the same subject could help assess pharmacokinetics noninvasively in preclinical studies.

2.1. Manganese-52

A potential candidate for immuno-PET application is ^{52}Mn ($t_{1/2}$ = 134.2 h), one of the lesser studied β^+-emitters at this time. Despite an attractive half-life, limited information is available with regard to the production and radiochemistry of ^{52}Mn. ^{52}Mn decays to a stable nuclide, but high abundance emission of the accompanying γ-ray (E_γ = 0.74 MeV, 90%) may add to radiation doses. Research on ^{52}Mn-labeled antibodies is effectively an untouched field because of its complex redox chemistry. Presently, Mn is generally studied as a contrast agent for MRI, and has been chelated with dipyridoxyl diphosphate, macrocyclic Schiff-base ligands, cyclopentadienide, and porphyrin derivatives [9]. Moreover, the present poor availability of the radionuclide impedes broad investigation or application of ^{52}Mn immuno-PET in current preclinical settings.

Due to the uptake in the intracellular space of the heart, $MnCl_2$ was employed in MRI studies of the ischemic heart and demonstrated its potential for detection of cell viability and the monitoring of calcium influx [15]. Based on the same mechanism, another Mn PET radionuclide, ^{52m}Mn ($t_{1/2}$ = 21 min) in the form of "free" radionuclide has been used in myocardial imaging in pigs [16]. In this study, ^{52m}Mn-PET data indicated high ratios of myocardium/lung and myocardium/blood; however, ^{52m}Mn failed to provide a quantitative evaluation of the heart during imaging because of prominent liver uptake [16]. Likewise, even when chelated, high liver uptake as well as bile, bowel, kidneys and pancreatic uptake were observed during a biodistribution study using ^{54}Mn-DTPA in dogs [17].

Mn is an essential trace element found in all human tissues, and is indispensable for maintaining normal physiological function [18]. Within the blood, the majority of Mn is bound to globulin and albumin [18]. Nonetheless, the blood retention of radiomanganese is low and does not significantly affect imaging quality [16,19] possibly due to rapid hepatobiliary clearance of Mn [20].

When administered intravenously, the bioavailability of Mn is much higher than that by oral administration (100% vs. 5%) [18]. The mass amount of radioactive Mn associated with radiolabeled Mn radiopharmaceuticals, being so small, is expected to be non-pharmacologic.

2.2. Cobalt-55

^{55}Co ($t_{1/2}$ = 17.5 h) decays with 76% abundance of β^+-emission (E_{max} = 1.50 MeV) and with a 95% abundance of γ-rays ($E\gamma$ = 931 keV). The favorable nuclear properties of ^{55}Co make it an interesting β^+-emitter for development of immuno-PET. Unfortunately, only a limited number of studies of ^{55}Co have been reported despite the large body of well defined chemistry of this metal ion.

Cobalt is well known to mimic calcium influx in ischemic or infarcted brain tissues. $^{55}CoCl_2$ has therefore been employed in PET imaging of cerebral damage in patients with stroke, atherosclerotic carotid artery disease, cerebral tumors and other brain injuries [21–23]. Compared to "old" cerebral infarcts (>2 months), ^{55}Co activity is higher in the ischemic tissues and can be used to image recent, recurrent infarcts [22]. Accordingly, it can be used to assess the age of brain infarction. In addition, ^{55}Co PET visualizes glioma successfully with respect to the location and size of the necrotic core of the tumor. This is based on the fact that calcium influx occurs during cell death and leukocyte activation as in necrosis [23]. The clearance of free ^{55}Co from blood is fast ($t_{1/2\alpha}$ = 1.0 min., $t_{1/2\beta}$ = 123 min), and becomes undetectable 3 days after injection, although some ^{55}Co ions might bind to leukocytes or other blood proteins [24]. Thus, while a high target-to-background ratio is expected due to rapid blood clearance and reduced background, ^{55}Co has also been reported to accumulate in the liver, kidney and bladder which could limit imaging applications [24].

Although ^{55}Co has thus far not been used to label intact mAbs, an anti-CEA antibody fragment was labeled with high yield and high stability via different bifunctional chelating agents such as cyclohexyl EDTA mono-anhydride, 4-isothiocyanato-*trans*-1,2,-diaminocyclohexane N,N,N',N'-tetraacetic acid and diethylenetriamine pentaacetic acid dianhydride [9]. In addition, small molecules such as ethylenediaminetetraacetic acid (EDTA) [25] and pendant carbohydrates [26] have been labeled. Interestingly, the biological half-life of ^{55}Co-EDTA is exceptionally short (<< 10 min). As a result, the main organs with high radioactivity are limited to heart, kidneys, and bladder [25]. In contrast to the above mentioned imaging using ^{55}Co ions, activity in the liver was not detectable by ^{55}Co-EDTA PET [25].

For the development of ^{55}Co immuno-PET, high abundance of high-energy γ-rays distinct from β^+-annihilation emissions, and long half-life of the daughter isotope ^{55}Fe ($t_{1/2}$ = 2.73 years) are major concerns [27].

2.3. Copper-64

^{64}Cu ($t_{1/2}$ = 12.7 h) is a β^+-emitting radioisotope for PET imaging and radiotherapy. Its decay is characterized by low probability (17.4 %) of β^+ emission, and a low β^+ energy (E_{max} = 656 keV) that is close to that of ^{18}F, along with a β^--emission ($E_{\beta\text{-}max}$ = 573 keV, 38.4%). Well-established coordination chemistry, as well as an attractive half-life, makes this radionuclide feasible for efficient labeling with a wide variety of biomolecules such as peptides, antibodies or nanoparticles. Thus far, a multitude of studies involving ^{64}Cu-labeled antibodies have been conducted preclinically, and demonstrate the potential application of this radionuclide for cancer detection, RIT dosing [28], pharmacokinetics [29], therapy planning and monitoring [30].

Success in cancer imaging and high specificity by ^{64}Cu immuno-PET has been demonstrated. As an example, ^{64}Cu-DOTA-cetuximab, which targets the extracellular domain of EGFR, accumulates preferably in xenografted EGFR-positive A431 tumors, but not EGFR-negative MDA-MB-435 tumors [31]. However, high blood activity is commonly seen in ^{64}Cu imaging [31,32] which might be related to the either slow clearance of intact antibodies as evidenced by the high percentage of intact ^{64}Cu-DOTA-cetuximab found in the blood within the 48 hour experimental period [31], or to radiotracer metabolism and transchelation due to the existence of circulating copper-binding proteins such as superoxide dismutase (SOD), ceruloplasmin, and albumin [33]. Either will result in excess activity remaining in the blood and contributing to background. A linear correlation was established between the expression of the target protein EGFR and tumor activity as measured by PET [34]. Nevertheless, an inconsistent result was obtained in a recent study [29]. In that report, a higher ^{64}Cu-DOTA-cetuximab accumulation was observed in low EGFR expressing UM-SCC-22B cells whereas low uptake was observed in high EGFR expressing SCC1 cells. Accordingly, UM-SCC-22B tumors were more responsive to ^{90}YDOTA-cetuximab RIT treatment than SCC1 tumors. Although it is unknown which factor breaks the linear rule, it was proposed that target expression alone might not be the dominant factor controlling tumor uptake *in vivo*, and that low microvessel density and poor vascular permeability might be the responsible factors [29]. This phenomenon of disparity is also observed using ^{89}Zr-labeled cetuximab, which shows the highest tumor-to-blood ratio in the xenografts with moderate expression of EGFR rather than the high expression tumor tissues [35].

One obstacle to clinical translation of ^{64}Cu immuno-PET is the significant liver uptake that might be associated with hepatobiliary excretion of copper and/or hepatic metabolism and transchelation. There are numerous proteins that bind copper in the liver such as Cu/Zn superoxide dismutase (Cu/Zn SOD), metallothionein, cytochrome c oxidase, etc. As a result, copper transchelation is anticipated in the liver after administration of ^{64}Cu probes. For example, ^{64}Cu-DOTA-cetuximab undergoes transchelation to proteins including SOD and metallothionein as early as 4 hours post-injection [31]. In tumor tissues, such extensive metabolism and transchelation also occur. In the blood which has a different protein population, ^{64}Cu-DOTA-cetuximab transchelates to metallothionein and other proteins, but not to SOD [31]. To reduce transchelation in liver, efforts continue to be made toward improving bifunctional chelates (BFCs) with the aim of binding ^{64}Cu to mAbs in a stable fashion under mild conditions with high yield [36]. DOTA is currently the most frequently used chelator because it is able to sequester a wide variety of isotopes. This is especially important for PET/RIT radionuclide pairs; thus, with the same immunoconjugate, radioimmunoimaging can guide RIT dosing and planning effectively and reliably. The Cu-

DOTA complex, however, is not highly stable *in vivo* and transchelation of ^{64}Cu often occurs, as mentioned above. Recently, multiple BFCs were investigated for their potential use in ^{64}Cu PET imaging, such as CHX-A"-DTPA, p-SCN-Bn-oxo-DO3A, p-SCN-Bn-PCTA, NOTA, and SarAr [36–38].

^{64}Cu is a residualizing radionuclide, and is often used for labeling of internalizing mAbs. After delivery into tumor cells by a specific antibody, ^{64}Cu tends to be retained in cells for long periods (Fig. 2). The characteristic of long retention is especially important for effective ^{64}Cu RIT of tumors. It is expected that a residualizing radionuclide has an advantage over a non-residualizing radiolabel with respect to RIT. Although this theory has been well developed and accepted [39–41], discrepant results were observed in a study of ^{64}Cu-labeled non-internalizing antibody, cT84.66, and an internalizing antibody, cBR96. Compared to ^{64}Cu-DOTA-cT84.66, ^{64}Cu-DOTA-cBR96 showed faster tumor accumulation, slower blood clearance, higher kidney uptake and slower clearance in the mononuclear phagocyte system (liver, spleen) in nude mice bearing LS174T colon carcinoma xenografts [42]. Interestingly, there was no significant difference in maximal radiotracer uptake [42], and RIT results [28] between ^{64}Cu-DOTA-cT84.66 and ^{64}Cu-DOTA-cBR96. Further mechanistic investigations are necessary to fully define the mechanisms involved.

A phase I/II clinical study has been performed with ^{64}Cu-labeled mAb 1A3 (^{64}Cu-TETA-1A3) in patients with suspected primary or advanced colorectal cancer [43]. The sensitivity of tumor localization by ^{64}Cu-TETA-1A3 was 71%. Concurrently, CT/MRI and FDG-PET were conducted to compare with ^{64}Cu PET imaging results. The superiority of ^{64}Cu-TETA-1A3 to CT/MRI was apparent for the detection of small foci (< 2 cm in diameter) with a sensitivity of 73% as compared to 20% by CT/MRI, but not as good as FDG-PET, whose sensitivity was 100%. Not surprisingly, there were challenges associated with detecting metastases in the lung and liver due to high hepatic uptake and slow blood clearance of the radiotracer. Probably due to these obstacles, there have been few clinical reports within the last decade using ^{64}Cu-labeled mAbs. Recently however, a ^{64}Cu-labeled peptide ^{64}Cu-DOTATATE, a ligand that targets the somatostatin receptor, was used in patients with neuroendocrine tumors [44]. At 1 and 3 hours after injection of ^{64}Cu-DOTATATE, high accumulation of radioactivity in the pituitary, adrenal glands, kidneys, renal pelvis, urinary bladder followed by moderate uptake in liver and spleen was observed. Tumors were visualized with high tumor-to-background ratios at 3 hours. After washout from most organs and lesions, retention of activity in the liver and intestines was obvious at 24 hours. The liver was the organ which received the highest radiation dose.

2.4. Gallium-66

^{66}Ga ($t_{1/2}$ = 9.4 h) is a β^+-emitter, which decays with high energy β^+ emission (E_{max} = 4.15 MeV, 56%) along with a mixture of high energy γ-ray emission (E_γ = 1.04 MeV, 37%). The labeling chemistry of gallium has been extensively studied due to the increasing popularity of ^{68}Ga ($t_{1/2}$ = 68 min) in PET imaging [45]. This provides advantages for the development of ^{66}Ga immuno-PET. However, the availability of ^{66}Ga is still limited although the production and separation of ^{66}Ga have been relatively well investigated [46].

A recent study reported a ^{66}Ga-labeled mAb, ^{66}Ga-NOTA-TRC105, which targets CD105/endoglin, for PET imaging of tumor angiogenesis in an animal model bearing murine 4T1 breast cancer xenografts [47]. It is well documented that the chelator NOTA can efficiently sequester radiogallium and produce an imaging agent with high *in vivo* stability [45]. During the 36 hour monitoring of the tumor uptake by serial PET imaging, ^{66}Ga-NOTA-TRC105 displayed high tumor uptake at the 20 and 36 hour time points (~9 %ID/g) with a tumor-to-muscle ratio of ~10 [47]. From the biodistribution study, persistent high activity in blood throughout the whole experimental period was evident, and moderate uptake of the

imaging probe was found in lung, liver, heart, kidney and spleen [47]. In addition, ^{66}Ga has also been used to label the small molecule, folate,[48] and a somatostatin peptide analogue [49], further demonstrating its feasibility in PET imaging of tumors.

When ^{66}Ga immuno-PET is under investigation, free ^{66}Ga from either impurities, or if released from unstable conjugates will accumulate preferably in bone and liver as demonstrated by intravenous administration of $^{66}GaCl_3$ into animals [49]. Although ^{67}Ga has been used in humans for imaging bone diseases since the 1950's [50], use of ^{66}Ga is not probable for future clinical applications. The high energy α^+- and γ-emissions are expected to produce reduced spatial resolution, poor image quality, and importantly, impose high radiation dose to both patients and personnel. These impractical characteristics impede its further clinical development despite its ready availability by cyclotron production.

2.5. Arsenic-72

^{72}As ($t_{1/2}$ = 25.9 h) is another β^+-emitter that has hitherto not been extensively studied. It decays with high abundance of β^+ emission (E_{max} = 2.5 MeV, 88%), and is an attractive radionuclide for PET imaging. The optimal method for production and purification of ^{72}As via a rapid and practical generator system remains under investigation [51,52]. Presently, ^{72}As can be generated either from a ^{72}Se/^{72}As generator system or cyclotron produced from a germanium target [53]. Because of the limited ^{72}As supply, research progress towards developing and evaluating ^{72}As continues to be slow and thereby impedes its further development towards translation to clinical settings.

Arsenic has a specific favorable chemical characteristic in that it can covalently bind to thiol groups. Based upon this advantage, biomolecules can be directly labeled with ^{72}As or after some chemical modification. For example, polymers based on *N*-(2-hydroxypropyl)-methacrylamide (HPMA) have been successfully labeled with $^{72/74}$As with minimal influence on polymer structure [54]. Thus far, ^{72}As has not been used to radiolabel mAbs. Instead, ^{74}As ($t_{1/2}$ = 17.8 days), has been used as a surrogate for ^{72}As to label an anti-phophatidylserine mAb, bavituximab, to visualize tumor vasculature in a rat model bearing prostate cancer xenografts [55]. In this study, bavituximab was first modified by succinimidyl acetylthioacetate (SATA) to introduce thiol-containing groups for use in covalently binding the radioarsenic to the protein. Result from an *in vitro* experiment demonstrated that ^{74}Asbavituximab was stable in serum during the experimental period (72 hours). From the PET imaging results, the highest tumor-to-background ratio was achieved 72 hours after administration of the imaging probe; and was accompanied by a high tumor-to-liver ratio (~22) as well.

2.6. Bromine-76

^{76}Br ($t_{1/2}$ = 16.2 h) is a radiohalogen that decays by β^+-emission (57%) with high production yield and reduced thyroid accumulation. Both properties make ^{76}Br an interesting alternative to ^{124}I (*vide infra*). However, unlike the large number of ^{124}I related studies reported, radiobromination techniques and biological behavior of ^{76}Br-labeled imaging agents have been far less investigated. Efforts are still focused on the development of effective and efficient production and radiolabeling methods of ^{76}Br [56–59].

Although the studies on ^{76}Br-labeled antibodies or fragments are limited, there is growing interest in its potential application for radioimmunoimaging because of the favorable long physical half-life. An immuno-PET study using a ^{76}Br-labeled anti-CEA mAb, 38S1, displayed the highest tumor uptake and good contrast at 2 days after injection in nude rats carrying subcutaneous human colon tumor xenografts [10,60]. It is encouraging to see that ^{76}Br-38S1 was superior to ^{18}F-FDG for imaging xenografted tumors; it exhibited higher

tumor-to-tissue ratios than ^{18}F-FDG [60] for many organs. In normal tissues, activity accumulated in the liver, lungs and part of the abdomen [60]. Therefore, the ratios of tumor-to-liver and tumor-to-lung were low in ^{76}Br-38S1 PET imaging.

Similar biodistribution results were observed in a recent study in which an antibody fragment L19-SIP, targeting fibronectin of tumor neovasculature, was labeled with ^{76}Br via an enzymatic approach (bromoperoxidase/H_2O_2) [61]. MicroPET/microCT imaging illustrated significant radioactivity in the abdominal area and blood-rich organs (such as lungs and heart) at 5 hours after injection. At 2 days post injection background activity decreased, and tumors were visible (SUV=2.4) together with left over activity in the stomach and bladder.

Slow blood clearance, resulting in increased background activity, appears to be a major obstacle to the use of ^{76}Br for radioimmunodiagnostics [10,60,61]. Low tumor-to-blood ratio was observed in both xenografted tumor models and liver metastasis models even at 2 days post-injection, the apparent optimal time point for ^{76}Br immuno-PET imaging [60]. The low ratio is attributed to a mechanism related to *in vivo* debromination of the radiotracer, although the radiobrominated antibodies or fragments were stable *in vitro* [10,61]. For example, only 25% of the intact ^{76}Br-L19-SIP was found in the serum, along with 21% residual immunoreactivity at 24 hours after injection while less than 1% of the intact antibody was detected in the urine sample. The majority of excreted activity was in the form of free ^{76}Br [61].

Direct administration of free radiobromide into animals facilitated an interpretation of the biodistribution characteristics of ^{76}Br-labeled proteins. Free bromide distributes rapidly into the extracellular space because of the negative membrane potential of living cells [62]. Slow renal clearance and persistent activity in blood were observed in biodistribution studies of free ^{76}Br [63,64]. In addition, accumulated activity was found in gastric mucosa [64], supporting the high stomach uptake of the radiotracer. In fact, free ^{76}Br was detected in serum at 2 hours after ^{76}Br-L19-SIP injection [61]. At 48 hours, the majority of radioactivity in the blood was free ^{76}Br. A similar phenomenon was observed for ^{125}I-L19-SIP [65], however, the free iodide cleared rapidly from blood and was taken up by the thyroid or excreted through the kidneys, resulting in low background uptake in non-target organs [66]. Further evidence was provided by the lower uptake of ^{125}I-38S1 compared with that of ^{76}Br-38S1 in tumors, blood and most normal tissues except thyroid at all examined time points from 2 to 46 hours [10]. Because of the faster excretion of ^{125}I, the concentration of ^{125}I in urine samples was three times higher than that of ^{76}Br during the first day [10]. Interestingly, ^{76}Br-labeled small molecules also released free bromide *in vivo* and showed high non-specific uptake in blood [67].

Because free ^{76}Br ions can be produced by either unstable labeling with radiobromide or by radiotracer metabolism after injection, the evaluation of radiotracer stability under simulated physiological conditions is critical before applying to animals. From all ^{76}Br immuno-PET studies reported thus far, poor systemic metabolic stability is a common problem that requires continued study.

Analogous to ^{124}I, ^{76}Br is non-residualizing (Fig. 2), contributing to poor cellular retention and slow excretion of bromide, and accordingly, reduced imaging contrast. The concept of “residualizing labels”, which cannot penetrate cellular membranes, is attractive and might be helpful if applied to improve the intracellular retention of radiohalogens. When an internalizing antibody, such as trastuzumab, is labeled with ^{76}Br, the radiometabolites are expected to be entrapped intracellularly after proteolytic degradation of the antibody in the

cells if measures are taken to allow residualization of the ^{76}Br [68]. Nevertheless, experiments need to be designed to verify the hypothesis using ^{76}Br-labeled antibodies.

To our knowledge, to date no radio-brominated antibody has been evaluated clinically. Due to the well-known distribution in extracellular space free ^{76}Br was employed to evaluate brain edema in brain tumor patients by PET [62]. Care should be taken, from a dosimetry point of view, when using ^{76}Br-labeled antibodies for staging and dosimetry support of clinical RIT. Due to the long biological half-life of bromide in the plasma of humans (~10 days) [69], physical decay would be the major manner of eliminating ^{76}Br-bromide from the body [62]. Low activity in normal organs (e.g., liver, brain) and blood would be an important criterion in the selection of a ^{76}Br radiotracer. It is noteworthy that administration of chloride was found beneficial in the elimination of bromide [70].

2.7. Yttrium-86

^{90}Y is now widely used in cancer radiotherapy. Due to the identical chemical form, ^{86}Y is an ideal imaging counterpart for patient selection and dosimetric calculations for ^{90}Y RIT. ^{86}Y ($t_{1/2}$ = 14.2 h) decays with high β^+ energy (E_{max} = 3.1 MeV, 33%) and 83% abundance of γ-emissions that significantly affect the image quality and recovery coefficients due to spurious coincidences. Fortunately, the image quality can be greatly improved when readily available and appropriate corrections are performed [71]. Stimulated by well-established chelation chemistry, ^{86}Y immuno-PET, has thus far demonstrated its potential in patient selection for targeted therapy, treatment monitoring, and dosimetric calculations for ^{90}Y-based RIT [72].

In our group, we have successfully labeled a number of approved antibodies with ^{86}Y and evaluated their potential use in PET imaging of target protein expression and RIT dosimetry in preclinical studies. These include bevacizumab [71], panitumumab [73,74], and cetuximab [75]. In these studies, a well-studied bifunctional chelate CHX-A" DTPA was conjugated to the antibody and used to sequester the radionuclide. As expected, organ uptake results from ^{86}Y immuno-PET were in good agreement with biodistribution studies [74,75] and all of these conjugates gave excellent image contrast at day 3 after injection of the imaging probe (Fig. 3); ^{86}Y-labeled panitumumab F(ab')$_2$ showed obvious tumors at day 1 [74]. The tumor-to-background ratios increased with time within the 3 day experimental period as a result of increased tumor uptake coupled with clearance of the probe from blood and liver.

In spite of high tumor uptake in both ^{86}Y-panitumumab and ^{86}Y-cetuximab (both bind to the HER1 receptor), significant differences were observed in blood and liver clearance rate in athymic mice bearing human mesothelioma xenografts [76]. ^{86}Y-cetuximab demonstrated a faster blood clearance with a $t_{1/2\alpha}$ of 0.9–1.1 hours compared to ^{86}Y-panitumumab with a $t_{1/2\alpha}$ of 2.6–3.1 hours. This might be explained by different affinities to Fc receptors of the chimeric IgG1 cetuximab and human IgG2 panitumumab [77]. Because the interaction of IgG and the Fc receptor is associated with the elimination of an antibody, the binding affinity of panitumumab to FcRn might be lower than that of cetuximab leading to slower first-phase blood clearance [76,77]. In addition, the liver clearance of ^{86}Y-cetuximab was slower than that of ^{86}Y-panitumumab, and therefore resulted in a lower tumor-to-liver ratio for ^{86}Y-cetuximab [76].

To date, there are no ^{86}Y-labeled antibodies reported for dosimetric assessment of RIT in humans. There are two drawbacks for ^{86}Y immuno-PET. One is the relatively short half-life compared with ^{90}Y; the other one is bone accumulation if ^{86}Y dissociates from unstable conjugates. A patient study, using a somatostatin analogue ^{86}Y-DOTA-DPhe1-Tyr3-octreotide (^{86}Y-DOTATOC) to monitor ^{90}Y-DOTATOC therapy, showed a slow uptake in

red marrow resulting in acute bone marrow toxicity. This might be related to ^{86}Y transchelation to transferrin proteins as demonstrated by an *in vitro* experiment using human plasma [78]. However, the detailed mechanism of the loss of ^{86}Y *in vivo* remains unclear with respect to whether this was an actual active transchelation, or a case of simple dissociation and loss of the radionuclide. Regardless, bone uptake is still a real concern and the use of stable chelation technology is an obvious requirement.

2.8. Zirconium-89

^{89}Zr has a favorable half-life ($t_{1/2}$ = 78.4 h), which is the longest among current commercially available β^+-emitting radiometals, and allows imaging up to 1 week after the injection of a ^{89}Zr-based probe. Its decay is characterized by high-abundance γ-rays (E_γ = 909 keV, 99.9%) and low-abundance β^+ (E_{max} = 897 keV, 22%) [79]. 89Zr immuno-PET, in this decade, has risen to the forefront and been successfully employed to assess target expression, *in vivo* biodistribution, and pharmacokinetics of antibodies in applications of cancer diagnosis, treatment planning and monitoring, and dosimetry [80–90]. Research on ^{89}Zr immuno-PET had been significantly hindered by complex and time consuming labeling methods and lack of availability of the radionuclide. With improvements in radiolabeling technology, antibodies can be labeled with ^{89}Zr efficiently and rapidly [80]. In addition, the availability of clinical grade ^{89}Zr for worldwide distribution fosters its popularization in clinical applications [81]. Thus far, multiple antibodies have been labeled with ^{89}Zr preclinically and clinically, such as HER1-targeted cetuximab [35,82] or panitumumab [83], HER2-targeted trastuzumab [81,84], VEGF-targeted bevacizumab [11,85], CD20-targeted ibritumomab tiuxetan [86], transforming growth factor-β (TGF-β)-targeted fresolimumab [87], CD105-targeted TRC105 [88], PSMA-targeted 7E11 [89], and others.

When a ^{89}Zr-labeled antibody is under investigation, a counterpart, using the same antibody labeled with ^{111}In, is usually employed for comparison of the uptake results as assessed by immuno-PET quantification and *ex vivo* biodistribution, while a ^{89}Zr-labeled IgG is generally used as a non-specific negative control [11,87]. In these studies blocking by an excess of unlabeled antibody is used to assess saturability and non-specific binding. By comparison with the robust consistency of ^{111}In-mAb biodistribution results, the reliability of the quantification of ^{89}Zr immuno-PET with agents, such as ^{89}Zr-bevacizumab [11], ^{89}Zr-trastuzumab [81] has been demonstrated. The specific targeting of ^{89}Z-rbevacizumab has been shown by its higher uptake in the tumor (~2 times) than that of human ^{89}Zr-IgG in SKOV-3 xenografts whereas a similar biodistribution pattern is observed in other organs except for kidneys [11]. An interesting result was obtained using ^{89}Zr-fresolimumab which targets TGF-β protein expression [87]. The uptake of ^{111}In-IgG was found to be comparable to that of ^{89}Zr-fresolimumab in primary tumors and metastases in addition to most organs. This can be explained by the characteristics of the target TGF-β. More than 90% of TGF-β is in its latent form, and not available to bind fresolimumab [87]. The difference between ^{89}Zr-fresolimumab and ^{111}In-IgG is in the liver, kidneys, and bone, suggesting high expression of active TGF-β, or an elevated occurrence of metabolism/excretion in these organs [87]. In addition, the stability of the ^{89}Zr probe is especially important because released ^{89}Zr tends to localize in the bone and may pose a significant risk to bone marrow. High bone uptake is observed in studies with both ^{89}Zr-fresolimumab and ^{89}Zr-bevacizumab [11,87]. The radioactivity in the bone has not yet been adequately analyzed to prove whether *in vivo* metal release or other mechanisms are involved.

A study with ^{89}Zr-panitumumab immuno-PET was recently conducted to quantitatively visualize HER1-expressing LS-174T human colon carcinoma in animal models bearing primary or metastatic tumors [83]. Primary tumor xenografts were shown with high contrast whereas tumors were not visualized in HER1-negative human melanoma A375 tumor

xenografts [83]. ^{89}Zr-panitumumab immuno-PET demonstrated the expression of HER1 in distant metastases in different animal models with intraperitoneal or pulmonary metastases. The peak tumor uptake was approximately 40 %ID/g at 3–4 d, 75 %ID/g at 2 d, and 95 %ID/g at 1–2 days after injection of the tracer for the subcutaneous, thoracic and intraperitoneal tumors, respectively [83]. This study therefore demonstrated the potential of ^{89}Zr-panitumumab immuno-PET for assessing HER1 status in distant metastases of colorectal cancer. The excellent tumor-to-background ratio might be related to the residualizing property of the radionuclide. This leads to low blood concentration and generally shows its superiority to radiohalogenmAbs with respect to tumor uptake. The radionuclide is retained in the target cells after internalization and degradation of the antibody probe (Fig. 2), as illustrated by the higher uptake of ^{89}Zr-cMAb U36 in tumor tissues compared to ^{124}I-cMAb U36 [2]. In another animal study using ^{89}Zr-fresolimumab, unfortunately, immuno-PET/micro-CT failed to detect breast cancer bone metastases, although bioluminescence imaging visualized tumors in multiple bone sites [87]. This might be due to the low expression of the lesions, unavailable target, or that the small bone metastases of the mice were beneath PET resolution. ^{89}Zr-bevacizumab PET also successfully monitored the antiangiogenic tumor response after heat shock protein 90 (HSP90) inhibition therapy in animal models [85]. ^{89}Zr-desferrioxamine B-7E11, as a marker of dying cells, was used to assess tumor response to therapy via binding to the intracellular epitope of PSMA [89].

Clinical studies have been performed using ^{89}Zr-trastuzumab in patients with HER2-positive metastatic breast cancer [84]. The clinical grade ^{89}Zr-trastuzumab was developed for clinical immuno-PET determination of HER2 expression, and was stable for up to 7 days in human serum [81]. Compared to ^{111}In-trastuzumab SPECT, ^{89}Zr-trastuzumab displayed superior image quality in spite of their similar biodistribution characteristics [81]. ^{89}Zr-trastuzumab immuno-PET visualized metastatic tumors in liver, lung, bone and brain 4–5 days after injection with excellent tumor uptake and image contrast. Decreased image quality was shown at day 6 or 7 after injection because of poor counting statistics [84]. From visual observation of the PET scan, the probe accumulates in liver, spleen, and kidney, but not lung, muscle, bone or brain. In this study, both a 50 mg dose for patients without trastuzumab therapy and a 10 mg dose for patients with trastuzumab treatment obtained excellent results. However, in patients without trastuzumab treatment, a 10 mg dose was not effective. This may be due to fast pharmacokinetics for lower concentrations of trastuzumab in blood [11,84].

^{89}Zr immuno-PET has been suggested to be promising for *in vivo* scouting and dosimetry predictions for ^{90}Y- and ^{177}Lu-RIT, which showed similar biodistribution characteristics except in bone in animal models [2,82]. In a recent clinical study, ^{89}Zr-ibritumomab tiuxetan PET (after coupling DFO to the mAb) was used to monitor biodistribution and estimate radiation dosimetry for ^{90}Y-ibritumomab tiuxetan in patients with relapsed B-cell non-Hodgkin's lymphoma scheduled for autologous stem cell transplantation [86]. Results showed that liver and spleen would be the organs with the highest ^{90}Y absorbed dose, followed by kidneys and lungs, and that there was no significant difference in the tumor absorbed doses between pre-therapy and therapy scans [86]. Moreover, results obtained from ^{89}ZrcmAb U36 PET also indicated that its highest absorbed dose in normal organ to be the liver followed by kidneys, thyroid, lungs, and spleen in patients with head and neck squamous cell carcinoma (HNSCC) [90].

Collectively, the dramatic progress in ^{89}Zr immuno-PET studies in recent years makes it a promising tool in radioimmunodiagnostics and therapy management that is very steadily progressing forward into what will be multiple clinical trials.

2.9. Iodine-124

^{124}I has been studied extensively in both experimental and clinical immuno-PET. Its physical half-life ($t_{1/2}$ = 100.2 h) is one of the longest among the currently available longer-lived β^+-emitting radionuclides suitable for PET. Accordingly, it has become possible to image antibody biodistribution over time scales of a week or more after administration. As one might expect given the extensive history of radioiodination, the radiolabeling chemistry of ^{124}I is well characterized; an antibody can be labeled with ^{124}I without loss of immunobiological activities [91,92]. Clinical grade ^{124}I is now commercially available for worldwide distribution [93]. Long physical half-life, together with well-investigated radiochemistry and biological behavior, makes ^{124}I an attractive label for preclinical and clinical PET studies.

Positron decay of ^{124}I is characterized by its high energy (E_{max} = 2.14 MeV), albeit low yield (23%), and the presence of a γ-ray emission (E_γ = 603 keV, 61%) in the same energy window as the annihilation photons [9,94]. These features of ^{124}I decay potentially pose several challenges to spatial resolution and high sensitivity during PET imaging. High energy results in a longer range of emitted β^+, and thus limits the image resolution; and higher scatter and random events are associated with higher background. ^{124}I-PET is therefore expected to have decreased image quality and challenging quantitative-analysis of the images as compared to some of the other longer-lived PET radionuclides. However, the development of hardware and software for data correction compensates for the interfering factors to a certain extent. For instance, optimization of the image reconstruction produces high-resolution PET images with reduced errors caused by γ-coincidences [95].

^{124}I immuno-PET has been, thus far, applied in cancer diagnosis [96,97], treatment planning [1,2] and monitoring [12], pharmacokinetics [12,98], and mechanistic studies. A large variety of proteins have been targeted, such as tumor associated glycoprotein (TAG)-72 [102], CA19-9 [101], carbonic anhydrase-IX (CA IX) [91,99,100,103], VEGF [12], A33 [96,97], CD22 [39], and ganglioside GD_2 [1]. Among the ^{124}I-labeled mAbs that are under development, ^{124}I-huA33 and ^{124}I-cG250 are in advanced clinical trials.

^{124}I-huA33, which recognizes and targets the A33 antigen in colorectal cancer, is used in patients with primary or metastatic colorectal cancer [96,97]. Quantitative PET localizes tumors with excellent tumor-to-background ratio at day 7, with about 20%–50% of A33 antigen in tumor tissue bound [96]. In spite of low activity in the liver and kidneys, the expression of A33 in normal colon and intestinal epithelial cells results in prominent uptake of the radiotracer in the intestines that might hinder tumor identification in some patients. Moreover, possible bowel toxicity needs to be considered although no significant toxicities have been observed with either a single dose of ^{124}I-huA33 [96] or RIT by infusion of ^{131}I-huA33 or ^{125}I-huA33 [104]. Importantly, a linear relationship exists between bound ^{124}I-huA33 and antigen expression [96] that sheds light on quantitative estimation of the molecular biomarker in diseased tissue for therapeutic regimen planning clinically.

CA IX is a biomarker for hypoxic tumor cells, and related to radiotherapeutic and chemotherapeutic resistance. ^{124}I-cG250 is applied for imaging of hypoxic tumors over-expressing CA IX in patients with clear cell renal cell carcinoma (ccRCC). The sensitivity and specificity for tumor detection have been reported as 94% and 100%, respectively, as demonstrated by PET/CT scanning of the abdominal region of patients from the xiphoid process to the pelvis [91]. A CA IX-negative tumor is highly associated with a less aggressive phenotype. On the basis of the correlation between PET/CT data and *in vitro* γ-counting of tumor tissues [99], ^{124}I-cG250 PET/CT has been suggested to quantify *in vivo* radioactivity uptake reliably. Current clinical data hold the potential for accurate pre-operative identification and intraoperative localization of ccRCC tumor tissues, and for

guiding complete tumor resection [91,103]. Thus far, no toxic effects have been found to be associated with this PET probe, at least within 4 weeks after surgery.

It is well known that ^{124}I is a non-residualizing label (Fig. 2). The major radiocatabolite of ^{124}I-labeled mAbs is monoiodotyrosine [39]. Unlike radio-metabolites from metal-labeled mAbs, monoiodotyrosine is lipophilic and can diffuse through lysosomal and cellular membranes. By virtue of the widespread deiodination enzymes in the body, iodotyrosine is further metabolized to free iodide as demonstrated by free ^{124}I found in urine after administration of ^{124}I-anti-TAG-72 mAbs [102]. As a result of cellular metabolism, tumor contrast is reduced in PET images, and tumor localization is generally lower than that using radiometal labels if the radioiodine is directly bound to tyrosine residues of mAb and there is any significant internalization of the mAb [39]. In an attempt to overcome this limitation, the introduction of a radioiodinated “residualizing group” to the internalizing proteins has been demonstrated to maintain ^{124}I intracellularly. This improved radiotracer uptake in target organs, and enhanced image contrast [39,105,106]. The advantages of applying the strategy of residualizing label is also illustrated by improvements in therapeutic efficacy of RIT as a result of enhanced retention time, higher tumor uptake, and absorbed radiation dose of the radiopharmaceutical compared to results from the agent with a non-residualizing iodine label [107].

^{124}I-labeled mAbs are suggested to be suitable for planning the therapeutic doses of ^{131}I- and ^{186}Re-labeled mAbs [2]. For example, to guide the treatment decisions in a phase I ^{131}I-3F8 RIT trial, ^{124}I-3F8 immuno-PET was used to evaluate a neuroblastoma patient [1]. In this study, the accumulated activity and retention time in tumor were measured to estimate the radiation absorbed dose from the radioiodinated antibodies. Due to the low uptake and unfavorable dosimetry in some bulky tumors in the patient, it was decided not to perform ^{131}I-3F8 RIT. It also needs to be considered that the effective predicted radiation dose by ^{124}I is ~20% higher than that of ^{131}I [95]; therefore, the administered dose needs to be adjusted accordingly.

As with all iodine radionuclides, ^{124}I is prone to accumulate in the thyroid. Efforts have been made to increase the *in vivo* stability of ^{124}I-labeled antibodies by using the *para*-iodophenyl (PIP) substituted conjugate [108]. While this reduces the thyroid radioiodine uptake, a more practical strategy in the clinic is to use oral iodine prior to the administration of an ^{124}I-PET reagent to minimize the the problem.

3. Regulatory affairs

In recent years, the continuing development of PET technology, novel radiopharmaceuticals, and federal reimbursement for FDG-PET in oncology, has spurred many new businesses, which are focused on PET imaging, clinically or academically. The limited production of radionuclides in universities or other institutions resulted in a trend towards distribution by centralized, for-profit facilities to satisfy clinical needs. Unlike short-lived radiopharmaceuticals, longer-lived radionuclides have the advantage of being delivered from remote commercial companies, thus decreases the need for manufacturing facilities at or close to the sites where the drugs are administered in patients. In the meantime, FDA regulatory control over the safety and efficacy of PET drugs has significantly increased. The guidance for current good manufacturing practice (cGMP) production of PET drugs was released in Aug. 2011 under the requirements of Section 121 of the Modernization Act. The guidance helps small businesses better understand and comply with the regulations, with respect to the recommendations in resources, procedures, and documentation for PET drug production to meet the requirements of cGMP standards coded in 21 CFR Part 212 and USP Chapter <823> published in 2009 [109]. CGMP is the minimum standard that ensures a drug

meets the requirements of safety and confirms its presented identity, strength, quality, and purity characteristics. However, this regulation targets and provides oversight for mainly short-lived PET radiopharmaceuticals and does not address long-lived radiotracers. With great hope, this content will be added in the near future.

4. Alternative strategies of PET radioimmunoimaging

Longer-lived positron emitters potentially pose risks to patients from long-term exposure of radiation dose especially in normal tissue sites of radioactivity accumulation. As aforementioned, slow blood clearance is frequently seen after administration of radiolabeled mAbs and other macromolecular agents. Antibody-based probes have the disadvantage of longer biodistribution times thereby limiting the sensitivity of the tracer during imaging. Alternative strategies have therefore been proposed and investigated. Here, we will briefly discuss pre-targeting approaches and various protein-engineering techniques.

4.1. Pre-targeting Approach

An intact antibody usually takes at least 2 days before achieving maximal tumor uptake while, at the same time, clearing from the non-targeted tissues occurs slowly [110]. To accommodate the slow pharmacodynamics of antibodies, a pre-targeting strategy has been proposed which allows a bispecific antibody (bsMAb) to accumulate maximally in the target before coupling with a radionuclide that is sequestered to a small molecule. Currently, there are multiple strategies for bsMAb/radio-peptide pairs, such as anti-hapten antibody/hapten, streptavidin antibody/biotin, oligonucleotide antibody/complementary oligonucleotide, and others [111]. In short, the targeting vector is permitted to bind to the cell surface target and, at an optimal time, a small radiolabeled moiety is administered that rapidly binds to the targeting vector. By virtue of its low molecular weight the small radiolabeled moiety is excreted very rapidly minimizing extravasation into or retention by normal tissues, thereby lowering background for imaging (and toxicity for therapy). In the case of a bsMAb, one binding arm of the antibody binds to the cell target while the other arm binds to the small radiolabeled moiety. Generally, an antibody clearing step is adopted before administration of the radiolabeled small molecule or peptide to remove unbound antibodies in the circulation thereby reducing both the background signal and unnecessary radiation exposure in non-target organs. In addition, a small, fast-clearing, radiolabeled peptide can be quickly captured by a pre-targeted tumor-associated bsMAbs. Thus, even short-lived PET radionuclides, such as ^{68}Ga, and ^{18}F, can be used. Because of the maximal tumor uptake and rapid targeting and clearance of the radionuclide, the tumor-to-background ratio is expected to be high. The pre-targeting approach has great potential for radioimmunodiagnosis and RIT. Efforts are being made to translate this strategy to clinical applications by Immunomedics, Inc, and others.

The pre-targeting strategy has been successfully applied in a mouse model bearing CEA-expressing LS174T human colonic xenografts [112]. In this study, a bispecific monoclonal anti-CEA/anti-hapten antibody was paired with a ^{68}Ga- or a ^{18}F-labeled hapten peptide, ^{68}Ga-IMP-288 or ^{18}F- IMP-449, with a 16 hour interval between administration of the two components. Imaging with either ^{68}Ga or ^{18}F displayed excellent imaging contrast 1 hour after injection of the radiopeptide. For example, the tumor uptake was ~10% ID/g for ^{68}Ga-IMP-288 and the tumor-to-blood ratio was ~70 [112]. Moreover, in a preliminary clinical trial, an anti-CEA/anti-DTPA bispecific antibody paired with an ^{111}In-di-DTPA peptide was employed in patients with primary colorectal cancer [113]. Among the intervals studied, the best imaging contrast was obtained with a 4 day interval, with resulting tumor-to-background ratios of 5.1 to 14.2 at 24 hours after injection of the radiolabeled peptide.

4.2. Protein-engineering

To overcome sustained blood accumulation and slow localization of intact antibodies, antibody-engineering techniques provide a tool to develop optimized immuno-PET radiotracers, which have a low hepatic uptake, and rapid clearance from blood and kidney. Ideally, these probes with a small molecular size would produce high-contrast images in a shorter time due to their rapid pharmacokinetics. A significant advantage is that it makes same day imaging possible. Currently, a multitude of antibody-based molecules have been engineered for PET imaging such as affibody (~10 kD), nanobody (~15 kD), single-chain variable fragment (scFv; ~25 kD), diabody (~50 kD), minibody (~80 kD), scFv-Fc (~105 kD), and others [8,114]. Because of the glomerular filtration barrier, larger proteins are excreted via liver (e.g., intact antibody, scFv-Fc, minibody); while smaller proteins are excreted via kidney (e.g., diabody, scFv, minibody, affibody) (Table 3).

Of the engineered proteins depicted in Table 3, the affibody and nanobody have the fastest clearance rates due to their small size. However, it is frequently found that higher contrast and faster imaging are achieved at the expense of tumor uptake. In a recent study, a ^{64}Cu-labeled EGFR-binding fibronectin domain ^{64}Cu-Fn$_{EI3.4.3'}$ (~10 kD) was assessed for PET imaging of EGFR in a xenograft mouse model [115]. Although it was characterized by a rapid accumulation of the probe in the tumor tissue (90% of the maximal uptake within 10 min), superior tumor to background ratio (~9 vs. ~2 for ^{64}Cu-DOTA-cetuximab [31]), lower liver uptake (~3.5% ID/g vs. ~15% ID/g for ^{64}Cu-DOTA-cetuximab [31]), and long retention in tumor, the maximal tumor uptake of the radiotracer was low (~3.4% ID/g vs. ~20% ID/g for ^{64}Cu-DOTA-cetuximab [31]). Similarly, an ^{124}I-labeled affibody Z$_{(HER2:342)}$ (~7 kD) identified tumors with a higher tumor-to-blood ratio compared to radioiodinated trastuzumab (16 vs. 1.2 at 24 hour, respectively), but exhibited a lower tumor uptake in xenograft-bearing mice [116]. Other disadvantages of the ^{64}Cu-Fn$_{EI3.4.3'}$ probe include high renal accumulation (~80% at 1 hour) and durable retention in kidney [115]. Accordingly, the kidney was potentially exposed to a high radiation dose over a long time. Indeed, this is also a common challenge in the development of small-sized, engineered antibodies for PET imaging. Numerous attempts have been made to modify the structure of the radiotracers to increase tumor uptake and decrease kidney uptake concurrently. For example, by altering the size of a diabody with a PEG component, a high tumor uptake (37.9% ID/g) was obtained with a PEG$_{48}$ conjugate at a later time point (44 hour) than with a smaller- or non-PEG diabody, along with a high tumor-to-background ratio [117]. Importantly, no interference from the kidneys was observed in PET imaging. It should also be noted that tumor retention and affinity might be associated with or influenced by the valency of the probes to the targeted antigen [118].

5. Future perspective and conclusions

Exhaustive understanding of the molecular biology of cancer and the discovery of new and specific cancer biomarkers as well as advances in antibody production and engineering techniques has spurred current advances in antibody development. This in turn has inspired novel immuno-PET probes. Meanwhile, increased availability of longer-lived positron-emitting radionuclides, along with improved radiolabeling methods, increases the flexibility of radioisotope selection to improve imaging quality.

Immuno-PET, characterized by non-invasive, real-time monitoring, holds promise for diagnostics and therapeutic management of cancer. Considering that there are more than 200 mAb candidates in clinical trials at varying phases of development for treatment of cancer and immunological diseases, the employment of immuno-PET would non-invasively define the *in vivo* behavior of the therapeutic mAbs and their interaction with the targets. Similarly, the impact of low molecular weight drugs on the various available cell surface targets could

equally be determined by monitoring response to therapy. Monitoring response non-invasively at the molecular level will undoubtedly assist the assessment of efficacy and safety, and speed up the drug-development process and its approval by FDA. Immuno-PET is also helpful in both the selection of candidate RIT patients and dosimetry for dose planning of RIT [105]. Examples of PET/RIT radionuclide pairs are $^{64}Cu/^{67}Cu$, $^{124}I/^{131}I$, $^{124}I/^{186}Re$, $^{124}I/^{188}Re$, $^{76}Br/^{131}I$, $^{86}Y/^{90}Y$, $^{89}Zr/^{177}Lu$, and $^{89}Zr/^{90}Y$ (Table 1) despite that some of the therapeutic radionuclides have intrinsic emissions suitable for γ- or SPECT imaging.

One caveat is the saturability of tracer uptake in tumor tissues when an antibody labeled with a positron emitter is applied to monitor the therapeutic effect of the same antibody drug. As observed in a PET study with ^{64}Cu-DOTA-conatumumab targeting to human death receptor 5, tumor uptake of the radiotracer substantially decreased with the co-injection of large amount of conatumumab [119]. Similar saturable uptake is also observed in spleen, but not in other tissues. In this circumstance, uptake of radiolabeled antibodies is expected to be lower if sufficient time is not allowed prior to the injection of the probe as compared to that without antibody treatment; and the results would not represent the actual value of the antigen expression of tumors.

To our knowledge, a relatively unexplored area in the study of immuno-PET is its potential application in monitoring circulating tumor cells (CTCs). It is well known that the number of CTCs grow with the progression of cancer whereby CTCs are recognized as a prognostic marker for cancer [120]. It has been demonstrated that higher numbers of CTCs are associated with more metastases sites as detected by ^{18}F-FDG PET/CT in patients with metastatic breast cancer [121]. It would, however, be more interesting if it were possible to evaluate and monitor the tumor cell load in peripheral blood with the sensitive PET imaging modality. An encouraging result shows the blood-pool activity from the left ventricle of the heart, as quantified by PET, is in a good agreement with that obtained from *ex vivo* activity counting [90]. We speculate that the total activity of the blood would be increased if sufficient CTCs are in the circulation.

To achieve images of high tumor-to-background ratio, as summarized in Fig. 4, it is essential to understand the properties of the selected targeting vector (e.g. antibody, fragments, peptides), the target antigen, and radiolabeling chemistry, particularly if it involves having to choose an appropriate chelator. The choice of appropriate longer-lived positron-emitting radionuclide for immuno-PET should be made judiciously for clinical applications. If an antibody, such as trastuzumab, cetuximab, or bevacizumab, rapidly internalizes into cells after antigen binding, a residualizing radionuclide, such as ^{64}Cu, ^{86}Y, or ^{89}Zr, is a better choice. As noted in section 2 (Fig. 2), ^{76}Br- and ^{124}I-labeled mAbs tend to release free radionuclides upon antibody internalization, resulting in rapid clearance of the radionuclides from the target tissue that creates higher background. In contrast, ^{64}Cu, which is residualizing, is trapped in lysosomes in cells after cellular metabolism of the ^{64}Cu-labeled mAbs, giving good image contrast. With respect to tumor location, if a PET probe has a high liver uptake in healthy subjects (for example, ^{64}Cu transchelation in liver), malignancies that are in the vicinity of liver cannot be detected reliably. In addition, it is also important to find the optimal imaging time point that shows low background and high tumor uptake. In sum, a radiopharmaceutical should be designed punctiliously, and all factors need to be carefully considered in order to get a high-quality image with minimal toxicity.

Acknowledgments

This work was supported by the Intramural Research Program of the National Institutes of Health (NIH), National Cancer Institute (NCI), and Center for Cancer Research (CCR). The contents of this article are solely the responsibility of the authors and do not necessarily represent the official views of the NIH, NCI or CCR.

Abbreviations

bsMAb	bispecific monoclonal antibody
CHX-A”-DTPA	*N*-[R-2-amino-3-(*p*-isothiocyanato-phenyl)propyl]-*trans*-(S,S)-cyclohexane-1,2-diamine-*N,N,N′,N”,N”*-pentaacetic acid
DOTA	1,4,7,10-tetraazacyclododecane-*N,N′,N”,N‴*-tetraacetic acid
DOTATOC	DOTA-DPhe1-Tyr3-octreotide
DTPA	diethylenetriaminepentaacetic acid
HPMA	*N*-(2-hydroxypropyl)-methacrylamide
NOTA	1,4,7-triazacyclononane-*N,N′,N”*-1,4,7-triacetic acid
PIB	*p*-iodobenzoate
PIP	*para*-iodophenyl
p-SCN-Bn-oxo-DO3A	1-oxa-4,7,1-tetraazacyclododecane-5-S-(4-isothiocyanatobenzyl)-4,7,10-triacetic acid
p-SCN-Bn-PCTA	3,6,9,15-tetraazabicyclo[9.3.1]-pentadeca-1(15),11,13-triene-4-S-(4-isothiocyanatobenzyl)-3,6,9-triacetic acid
SarAr	1-*N*-(4-aminobenzyl)-3,6,10,13,16,19-hexaazabicyclo[6.6.6]eicosane-1,8-diamine
SATA	succinimidyl acetylthioacetate

References

[1]. Larson SM, Pentlow KS, Volkow ND, Wolf AP, Finn RD, Lambrecht RM, Graham MC, Di Resta G, Bendriem B, Daghighian F, Yeh SDJ, Wang GJ, Cheung NV. PET scanning of iodine-124-3F8 as an approach to tumor dosimetry during treatment planning for radioimmunotherapy in a child with neuroblastoma. J. Nucl. Med. 1992; 33:2020–2023. [PubMed: 1432165]

[2]. Verel I, Visser GW, Boerman OC, van Eerd JE, Finn R, Boellaard R, Vosjan MJ, Stigter-van Walsum M, Snow GB, van Dongen GA. Long-lived positron emitters zirconium-89 and iodine-124 for scouting of therapeutic radioimmunoconjugates with PET. Cancer Biother. Radiopharm. 2003; 18:655–661. [PubMed: 14503961]

[3]. Gambhir SS, Czernin J, Schwimmer J, Silverman DH, Coleman RE, Phelps ME. A tabulated summary of the FDG PET literature. J. Nucl. Med. 2001; 42:1S–93S. [PubMed: 11483694]

[4]. http://en.wikipedia.org/wiki/Monoclonal_antibody_therapy

[5]. Boswell CA, Brechbiel MW. Development of radioimmunotherapeutic and diagnostic antibodies: an inside-out view. Nucl. Med. Biol. 2007; 34:757–778. [PubMed: 17921028]

[6]. McBride WJ, Sharkey RM, Karacay H, D'Souza CA, Rossi EA, Laverman P, Chang CH, Boerman OC, Goldenberg DM. A novel method of ^{18}F radiolabeling for PET. J. Nucl. Med. 2009; 50:991–998. [PubMed: 19443594]

[7]. Dijkgraaf I, Franssen GM, McBride WJ, D'Souza CA, Laverman P, Smith CJ, Goldenberg DM, Oyen WJ, Boerman OC. PET of tumors expressing gastrin-releasing peptide receptor with an ^{18}F-labeled bombesin analog. J. Nucl. Med. 2012; 53:947–952. [PubMed: 22570329]

[8]. McCabe KE, Wu AM. Positive progress in immunoPET--not just a coincidence. Cancer Biother. Radiopharm. 2010; 25:253–261. [PubMed: 20578830]

[9]. Nayak TK, Brechbiel MW. Radioimmunoimaging with longer-lived positron-emitting radionuclides: potentials and challenges. Bioconjug Chem. 2009; 20:825–841. [PubMed: 19125647]

[10]. Lövqvist A, Sundin A, Ahlström H, Carlsson J, Lundqvist H. Pharmacokinetics and experimental PET imaging of a bromine-76-labeled monoclonal anti-CEA antibody. J. Nucl. Med. 1997; 38:395–401. [PubMed: 9074527]

[11]. Nagengast WB, de Vries EG, Hospers GA, Mulder NH, de Jong JR, Hollema H, Brouwers AH, van Dongen GA, Perk LR, Lub-de Hooge MN. *In vivo* VEGF imaging with radiolabeled bevacizumab in a human ovarian tumor xenograft. J. Nucl. Med. 2007; 48:1313–1319. [PubMed: 17631557]

[12]. Jayson GC, Zweit J, Jackson A, Mulatero C, Julyan P, Ranson M, Broughton L, Wagstaff J, Hakannson L, Groenewegen G, Bailey J, Smith N, Hastings D, Lawrance J, Haroon H, Ward T, McGown AT, Tang M, Levitt D, Marreaud S, Lehmann FF, Herold M, Zwierzina H. Molecular imaging and biological evaluation of HuMV833 anti-VEGF antibody: implications for trial design of antiangiogenic antibodies. J. Natl. Cancer Inst. 2002; 94:1484–1493. [PubMed: 12359857]

[13]. Benz MR, Evilevitch V, Allen-Auerbach MS, Eilber FC, Phelps ME, Czernin J, Weber WA. Treatment monitoring by ^{18}F-FDG PET/CT in patients with sarcomas: interobserver variability of quantitative parameters in treatment-induced changes in histopathologically responding and nonresponding tumors. J. Nucl. Med. 2008; 49:1038–1046. [PubMed: 18552153]

[14]. Hatt M, Cheze-le Rest C, van Baardwijk A, Lambin P, Pradier O, Visvikis D. Impact of tumor size and tracer uptake heterogeneity in ^{18}F-FDG PET and CT non-small cell lung cancer tumor delineation. J. Nucl. Med. 2011; 52:1690–1697. [PubMed: 21990577]

[15]. Hu TC, Christian TF, Aletras AH, Taylor JL, Koretsky AP, Arai AE. Manganese enhanced magnetic resonance imaging of normal and ischemic canine heart. Magn. Reson. Med. 2005; 54:196–200. [PubMed: 15968667]

[16]. Buck A, Nguyen N, Burger C, Ziegler S, Frey L, Weigand G, Erhardt W, Senekowitsch-Schmidtke R, Pellikka R, Bläuenstein P, Locher JT, Schwaiger M. Quantitative evaluation of manganese-52m as a myocardial perfusion tracer in pigs using positron emission tomography. Eur. J. Nucl. Med. 1996; 23:1619–1627. [PubMed: 8929316]

[17]. Boudreau RJ, Burbidge S, Sirr S, Loken MK. Comparison of the biodistribution of manganese-54 DTPA and gadolinium-153 DTPA in dogs. J. Nucl. Med. 1987; 28:349–353. [PubMed: 3819851]

[18]. Aschner M, Erikson KM, Dorman DC. Manganese dosimetry: species differences and implications for neurotoxicity. Crit. Rev. Toxicol. 2005; 35:1–32. [PubMed: 15742901]

[19]. Schroeter JD, Nong A, Yoon M, Taylor MD, Dorman DC, Andersen ME, Clewell HJ 3rd. Analysis of manganese tracer kinetics and target tissue dosimetry in monkeys and humans with multi-route physiologically based pharmacokinetic models. Toxicol. Sci. 2011; 120:481–498. [PubMed: 21205636]

[20]. Cikrt M. Biliary excretion of ^{203}Hg, ^{64}Cu, ^{52}Mn, and ^{210}Pb in the rat. Br. J. Ind. Med. 1972; 29:74–80. [PubMed: 5060249]

[21]. De Reuck J, Paemeleire K, Santens P, Strijckmans K, Lemahieu I. Cobalt-55 positron emission tomography in symptomatic atherosclerotic carotid artery disease: borderzone versus territorial infarcts. Clin. Neurol. Neurosurg. 2004; 106:77–81. [PubMed: 15003294]

[22]. De Reuck J, Santens P, Keppens J, De Bleecker J, Strijckmans K, Goethals P, Lemahieu I, Korf J. Cobalt-55 positron emission tomography in recurrent ischaemic stroke. Clin. Neurol. Neurosurg. 1999; 101:15–18. [PubMed: 10350197]

[23]. Jansen HM, Dierckx RA, Hew JM, Paans AM, Minderhoud JM, Korf J. Positron emission tomography in primary brain tumours using cobalt-55. Nucl. Med. Commun. 1997; 18:734–740. [PubMed: 9293504]

[24]. Jansen HM, Knollema S, van der Duin LV, Willemsen AT, Wiersma A, Franssen EJ, Russel FG, Korf J, Paans AM. Pharmacokinetics and dosimetry of cobalt-55 and cobalt-57. J. Nucl. Med. 1996; 37:2082–2086. [PubMed: 8970539]

[25]. Goethals P, Volkaert A, Vandewielle C, Dierckx R, Lameire N. ^{55}Co-EDTA for renal imaging using positron emission tomography (PET): a feasibility study. Nucl. Med. Biol. 2000; 27:77–81. [PubMed: 10755649]

[26]. Ferreira CL, Lapi S, Steele J, Green DE, Ruth TJ, Adam MJ, Orvig C. ^{55}Cobalt complexes with pendant carbohydrates as potential PET imaging agents. Appl. Radiat. Isot. 2007; 65:1303–1308. [PubMed: 17666190]

[27]. Hao G, Singh AN, Liu W, Sun X. PET with non-standard nuclides. Curr. Top. Med. Chem. 2010; 10:1096–1112. [PubMed: 20388114]

[28]. Bryan JN, Jia F, Mohsin H, Sivaguru G, Anderson CJ, Miller WH, Henry CJ, Lewis MR. Monoclonal antibodies for copper-64 PET dosimetry and radioimmunotherapy. Cancer Biol. Ther. 2011; 11:1001–1007. [PubMed: 21464612]

[29]. Niu G, Sun X, Cao Q, Courter D, Koong A, Le QT, Gambhir SS, Chen X. Cetuximab-based immunotherapy and radioimmunotherapy of head and neck squamous cell carcinoma. Clin. Cancer Res. 2010; 16:2095–2105. [PubMed: 20215534]

[30]. Evans MJ, Smith-Jones PM, Wongvipat J, Navarro V, Kim S, Bander NH, Larson SM, Sawyers CL. Noninvasive measurement of androgen receptor signaling with a positron-emitting radiopharmaceutical that targets prostate-specific membrane antigen. Proc. Natl. Acad. Sci. U. S. A. 2011; 108:9578–9582. [PubMed: 21606347]

[31]. Li WP, Meyer LA, Capretto DA, Sherman CD, Anderson CJ. Receptor-binding, biodistribution, and metabolism studies of ^{64}Cu-DOTA-cetuximab, a PET-imaging agent for epidermal growth-factor receptor-positive tumors. Cancer Biother. Radiopharm. 2008; 23:158–171. [PubMed: 18454685]

[32]. Elsässer-Beile U, Reischl G, Wiehr S, Bühler P, Wolf P, Alt K, Shively J, Judenhofer MS, Machulla HJ, Pichler BJ. PET imaging of prostate cancer xenografts with a highly specific antibody against the prostate-specific membrane antigen. J. Nucl. Med. 2009; 50:606–611. [PubMed: 19289418]

[33]. Mirick GR, O'Donnell RT, DeNardo SJ, Shen S, Meares CF, DeNardo GL. Transfer of copper from a chelated ^{67}Cu-antibody conjugate to ceruloplasmin in lymphoma patients. Nucl. Med. Biol. 1999; 26:841–845. [PubMed: 10628566]

[34]. Cai W, Chen K, He L, Cao Q, Koong A, Chen X. Quantitative PET of EGFR expression in xenograft-bearing mice using ^{64}Cu-labeled cetuximab, a chimeric anti-EGFR monoclonal antibody. Eur. J. Nucl. Med. Mol. Imaging. 2007; 34:850–858. [PubMed: 17262214]

[35]. Aerts HJ, Dubois L, Perk L, Vermaelen P, van Dongen GA, Wouters BG, Lambin P. Disparity between *in vivo* EGFR expression and ^{89}Zr-labeled cetuximab uptake assessed with PET. J. Nucl. Med. 2009; 50:123–131. [PubMed: 19091906]

[36]. Cooper MS, Ma MT, Sunassee K, Shaw KP, Williams JD, Paul RL, Donnelly PS, Blower PJ. Comparison of ^{64}Cu-complexing bifunctional chelators for radioimmunoconjugation: labeling efficiency, specific activity, and *in vitro/in vivo* stability. Bioconjug. Chem. 2012 [Epub ahead of print].

[37]. Zhang Y, Hong H, Engle JW, Bean J, Yang Y, Leigh BR, Barnhart TE, Cai W. Positron emission tomography imaging of CD105 expression with a ^{64}Cu-labeled monoclonal antibody: NOTA is superior to DOTA. PLoS One. 2011; 6:e28005. [PubMed: 22174762]

[38]. Dearling JL, Voss SD, Dunning P, Snay E, Fahey F, Smith SV, Huston JS, Meares CF, Treves ST, Packard AB. Imaging cancer using PET--the effect of the bifunctional chelator on the biodistribution of a ^{64}Cu-labeled antibody. Nucl. Med. Biol. 2011; 38:29–38. [PubMed: 21220127]

[39]. Sharkey RM, Behr TM, Mattes MJ, Stein R, Griffiths GL, Shih LB, Hansen HJ, Blumenthal RD, Dunn RM, Juweid ME, Goldenberg DM. Advantage of residualizing radiolabels for an internalizing antibody against the B-cell lymphoma antigen. CD22. Cancer Immunol. Immunother. 1997; 44:179–188.

[40]. Baranowska-Kortylewicz J, Kortylewicz ZP, Hoffman D, Dalrymple GV. Prodrugs in site-selective delivery of radiopharmaceuticals. Q. J. Nucl. Med. 1997; 41:127–139. [PubMed: 9203852]

[41]. Thorpe SR, Baynes JW, Chroneos ZC. The design and application of residualizing labels for studies of protein catabolism. FASEB J. 1993; 7:399–405. [PubMed: 8462781]

[42]. Bryan JN, Jia F, Mohsin H, Sivaguru G, Miller WH, Anderson CJ, Henry CJ, Lewis MR. Comparative uptakes and biodistributions of internalizing vs. noninternalizing copper-64

radioimmunoconjugates in cell and animal models of colon cancer. Nucl. Med. Biol. 2005; 32:851–858. [PubMed: 16253810]

[43]. Philpott GW, Schwarz SW, Anderson CJ, Dehdashti F, Connett JM, Zinn KR, Meares CF, Cutler PD, Welch MJ, Siegel BA. RadioimmunoPET: detection of colorectal carcinoma with positron-emitting copper-64-labeled monoclonal antibody. J. Nucl. Med. 1995; 36:1818–1824. [PubMed: 7562049]

[44]. Pfeifer A, Knigge U, Mortensen J, Oturai P, Berthelsen AK, Loft A, Binderup T, Rasmussen P, Elema D, Klausen TL, Holm S, von Benzon E, Højgaard L, Kjaer A. Clinical PET of neuroendocrine tumors using ^{64}Cu-DOTATATE: first-in-humans study. J. Nucl. Med. 2012 [Epub ahead of print] doi:10.2967/jnumed.111.101469.

[45]. Velikyan I. Positron emitting ^{68}Ga-based imaging agents: chemistry and diversity. Med. Chem. 2011; 7:345–379. [PubMed: 21711223]

[46]. Lewis MR, Reichert DE, Laforest R, Margenau WH, Shefer RE, Klinkowstein RE, Hughey BJ, Welch MJ. Production and purification of gallium-66 for preparation of tumor-targeting radiopharmaceuticals. Nucl. Med. Biol. 2002; 29:701–706. [PubMed: 12234596]

[47]. Engle JW, Hong H, Zhang Y, Valdovinos HF, Myklejord DV, Barnhart TE, Theuer CP, Nickles RJ, Cai W. Positron emission tomography imaging of tumor angiogenesis with a ^{66}Ga-labeled monoclonal antibody. Mol. Pharm. 2012; 9:1441–1448. [PubMed: 22519890]

[48]. Mathias CJ, Lewis MR, Reichert DE, Laforest R, Sharp TL, Lewis JS, Yang ZF, Waters DJ, Snyder PW, Low PS, Welch MJ, Green MA. Preparation of ^{66}Ga- and ^{68}Ga-labeled Ga(III)-deferoxamine-folate as potential folate-receptor-targeted PET radiopharmaceuticals. Nucl. Med. Biol. 2003; 30:725–731. [PubMed: 14499330]

[49]. Ugur O, Kothari PJ, Finn RD, Zanzonico P, Ruan S, Guenther I, Maecke HR, Larson SM. Ga-66 labeled somatostatin analogue DOTA-DPhe1-Tyr3-octreotide as a potential agent for positron emission tomography imaging and receptor mediated internal radiotherapy of somatostatin receptor positive tumors. Nucl. Med. Biol. 2002; 29:147–157. [PubMed: 11823119]

[50]. Van Der Werff JT. Clinical investigations on the use of radioactive gallium (Ga66 and Ga67) in bone diseases. Acta radiol. 1954; 41:343–347. [PubMed: 13158135]

[51]. Ballard B, Wycoff D, Birnbaum ER, John KD, Lenz JW, Jurisson SS, Cutler CS, Nortier FM, Taylor WA, Fassbender ME. Selenium-72 formation via ^{nat}Br(p,x) induced by 100 MeV protons: steps towards a novel ^{72}Se/^{72}As generator system. Appl. Radiat. Isot. 2012; 70:595–601. [PubMed: 22326368]

[52]. Chajduk E, Doner K, Polkowska-Motrenko H, Bilewicz A. Novel radiochemical separation of arsenic from selenium for ^{72}Se/^{72}As generator. Appl. Radiat. Isot. 2012; 70:819–822. [PubMed: 22342310]

[53]. Ballard B, Nortier FM, Birnbaum ER, John KD, Phillips DR, Fassbender ME. Radioarsenic from a Portable ^{72}Se/^{72}As Generator: A Current Perspective. Curr. Radiopharm. 2012; 5:264–270. [PubMed: 22697482]

[54]. Herth MM, Barz M, Jahn M, Zentel R, Rösch F. $^{72/74}$As-labeling of HPMA based polymers for long-term in vivo PET imaging. Bioorg. Med. Chem. Lett. 2010; 20:5454–5458. [PubMed: 20709549]

[55]. Jennewein M, Lewis MA, Zhao D, Tsyganov E, Slavine N, He J, Watkins L, Kodibagkar VD, O'Kelly S, Kulkarni P, Antich PP, Hermanne A, Rösch F, Mason RP, Thorpe PE. Vascular imaging of solid tumors in rats with a radioactive arsenic-labeled antibody that binds exposed phosphatidylserine. Clin. Cancer Res. 2008; 14:1377–1385. [PubMed: 18316558]

[56]. Zhou D, Zhou H, Jenks CC, Lewis JS, Katzenellenbogen JA, Welch MJ. Bromination from the macroscopic level to the tracer radiochemical level: ^{76}Br radiolabeling of aromatic compounds via electrophilic substitution. Bioconjug. Chem. 2009; 20:808–816. [PubMed: 19260733]

[57]. Lang L, Li W, Jia HM, Fang DC, Zhang S, Sun X, Zhu L, Ma Y, Shen B, Kiesewetter DO, Niu G, Chen X. New methods for labeling RGD peptides with bromine-76. Theranostics. 2011; 1:341–353. [PubMed: 21938262]

[58]. Aslam MN, Sudár S, Hussain M, Malik AA, Qaim SM. Evaluation of excitation functions of proton, ^{3}He- and α-particle induced reactions for production of the medically interesting positron-emitter bromine-76. Appl. Radiat. Isot. 2011; 69:1490–1505. [PubMed: 21723137]

[59]. Mume E, Orlova A, Malmström PU, Lundqvist H, Sjöberg S, Tolmachev V. Radiobromination of humanized anti-HER2 monoclonal antibody trastuzumab using N-succinimidyl 5-bromo-3-pyridinecarboxylate, a potential label for immuno-PET. Nucl. Med. Biol. 2005; 32:613–622. [PubMed: 16026708]

[60]. Lövqvist A, Sundin A, Roberto A, Ahlström H, Carlsson J, Lundqvist H. Comparative PET imaging of experimental tumors with bromine-76-labeled antibodies, fluorine-18-fluorodeoxyglucose and carbon-11-methionine. J. Nucl. Med. 1997; 38:1029–1035. [PubMed: 9225786]

[61]. Rossin R, Berndorff D, Friebe M, Dinkelborg LM, Welch MJ. Small-animal PET of tumor angiogenesis using a ^{76}Br-labeled human recombinant antibody fragment to the ED-B domain of fibronectin. J. Nucl. Med. 2007; 48:1172–1179. [PubMed: 17574989]

[62]. Bruehlmeier M, Roelcke U, Bläuenstein P, Missimer J, Schubiger PA, Locher JT, Pellikka R, Ametamey SM. Measurement of the extracellular space in brain tumors using ^{76}Br-bromide and PET. J. Nucl. Med. 2003; 44:1210–1218. [PubMed: 12902409]

[63]. Lee H, Finck BN, Jones LA, Welch MJ, Mach RH. Synthesis and evaluation of a bromine-76-labeled PPARγ antagonist 2-bromo-5-nitro-N-phenylbenzamide. Nucl. Med. Biol. 2006; 33:847–854. [PubMed: 17045164]

[64]. Soremark R, Ullberg S. Distribution of bromide in mice: an autoradiographic study with Br-82. Int. J. Appl. Radiat. Isot. 1960; 8:192–197.

[65]. Borsi L, Balza E, Bestagno M, Castellani P, Carnemolla B, Biro A, Leprini A, Sepulveda J, Burrone O, Neri D, Zardi L. Selective targeting of tumoral vasculature: comparison of different formats of an antibody (L19) to the ED-B domain of fibronectin. Int. J. Cancer. 2002; 102:75–85. [PubMed: 12353237]

[66]. Lövqvist A, Sundin A, Ahlström H, Carlsson J, Lundqvist H. Pharmacokinetics and experimental PET imaging of a bromine-76-labeled monoclonal anti-CEA antibody. J. Nucl. Med. 1997; 38:395–401. [PubMed: 9074527]

[67]. Zhou D, Sharp TL, Fettig NM, Lee H, Lewis JS, Katzenellenbogen JA, Welch MJ. Evaluation of a bromine-76-labeled progestin 16α,17α-dioxolane for breast tumor imaging and radiotherapy: *in vivo* biodistribution and metabolic stability studies. Nucl. Med. Biol. 2008; 35:655–663. [PubMed: 18678350]

[68]. Tolmachev V, Orlova A. Influence of labelling methods on biodistribution and imaging properties of radiolabelled peptides for visualisation of molecular therapeutic targets. Curr. Med. Chem. 2010; 17:2636–2655. [PubMed: 20491631]

[69]. Vaiseman N, Koren G, Pencharz P. Pharmacokinetics of oral and intravenous bromide in normal volunteers. J. Toxicol. Clin. Toxicol. 1986; 24:403–413. [PubMed: 3783804]

[70]. Rauws AG, Van Logten MJ. The influence of dietary chloride on bromide excretion in the rat. Toxicology. 1975; 3:29–32. [PubMed: 1121704]

[71]. Nayak TK, Garmestani K, Baidoo KE, Milenic DE, Brechbiel MW. PET imaging of tumor angiogenesis in mice with VEGF-A-targeted ^{86}Y-CHX-A“-DTPA-bevacizumab. Int. J. Cancer. 2011; 128:920–926. [PubMed: 20473899]

[72]. Nayak TK, Brechbiel MW. ^{86}Y based PET radiopharmaceuticals: radiochemistry and biological applications. Med. Chem. 2011; 7:380–388. [PubMed: 21711222]

[73]. Wong KJ, Baidoo KE, Nayak TK, Garmestani K, Brechbiel MW, Milenic DE. *In vitro* and *in vivo* pre-clinical analysis of a F(ab')$_2$ fragment of panitumumab for molecular imaging and therapy of HER1-positive cancers. EJNMMI Res. 2011; 1:1. [PubMed: 21845232]

[74]. Nayak TK, Garmestani K, Baidoo KE, Milenic DE, Brechbiel MW. Preparation, biological evaluation, and pharmacokinetics of the human anti-HER1 monoclonal antibody panitumumab labeled with ^{86}Y for quantitative PET of carcinoma. J. Nucl. Med. 2010; 51:942–950. [PubMed: 20484421]

[75]. Nayak TK, Regino CA, Wong KJ, Milenic DE, Garmestani K, Baidoo KE, Szajek LP, Brechbiel MW. PET imaging of HER1-expressing xenografts in mice with ^{86}Y-CHX-A“-DTPA-cetuximab. Eur. J. Nucl. Med. Mol. Imaging. 2010; 37:1368–1376. [PubMed: 20155263]

[76]. Nayak TK, Garmestani K, Milenic DE, Baidoo KE, Brechbiel MW. HER1-targeted ^{86}Y-panitumumab possesses superior targeting characteristics than ^{86}Y-cetuximab for PET imaging

of human malignant mesothelioma tumors xenografts. PLoS One. 2011; 6:e18198. [PubMed: 21464917]

[77]. Wang W, Wang EQ, Balthasar JP. Monoclonal antibody pharmacokinetics and pharmacodynamics. Clin. Pharmacol. Ther. 2008; 84:548–558. [PubMed: 18784655]

[78]. Walrand S, Barone R, Pauwels S, Jamar F. Experimental facts supporting a red marrow uptake due to radiometal transchelation in ^{90}Y-DOTATOC therapy and relationship to the decrease of platelet counts. Eur. J. Nucl. Med. Mol. Imaging. 2011; 38:1270–1280. [PubMed: 21318451]

[79]. Zhang Y, Hong H, Cai W. PET tracers based on Zirconium-89. Curr. Radiopharm. 2011; 4:131–139. [PubMed: 22191652]

[80]. Vosjan MJ, Perk LR, Visser GW, Budde M, Jurek P, Kiefer GE, van Dongen GA. Conjugation and radiolabeling of monoclonal antibodies with zirconium-89 for PET imaging using the bifunctional chelate p-isothiocyanatobenzyl-desferrioxamine. Nat. Protoc. 2010; 5:739–743. [PubMed: 20360768]

[81]. Dijkers EC, Kosterink JG, Rademaker AP, Perk LR, van Dongen GA, Bart J, de Jong JR, de Vries EG, Lub-de Hooge MN. Development and characterization of clinical-grade ^{89}Zr-trastuzumab for HER2/neu immunoPET imaging. J. Nucl. Med. 2009; 50:974–981. [PubMed: 19443585]

[82]. Perk LR, Visser GW, Vosjan MJ, Stigter-van Walsum M, Tijink BM, Leemans CR, van Dongen GA. ^{89}Zr as a PET surrogate radioisotope for scouting biodistribution of the therapeutic radiometals ^{90}Y and ^{177}Lu in tumor-bearing nude mice after coupling to the internalizing antibody cetuximab. J. Nucl. Med. 2005; 46:1898–1906. [PubMed: 16269605]

[83]. Nayak TK, Garmestani K, Milenic DE, Brechbiel MW. PET and MRI of metastatic peritoneal and pulmonary colorectal cancer in mice with human epidermal growth factor receptor 1-targeted ^{89}Zr-labeled panitumumab. J. Nucl. Med. 2012; 53:113–120. [PubMed: 22213822]

[84]. Dijkers EC, Oude Munnink TH, Kosterink JG, Brouwers AH, Jager PL, de Jong JR, van Dongen GA, Schröder CP, Lub-de Hooge MN, de Vries EG. Biodistribution of ^{89}Zrtrastuzumab and PET imaging of HER2-positive lesions in patients with metastatic breast cancer. Clin. Pharmacol. Ther. 2010; 87:586–592. [PubMed: 20357763]

[85]. Nagengast WB, de Korte MA, Oude Munnink TH, Timmer-Bosscha H, den Dunnen WF, Hollema H, de Jong JR, Jensen MR, Quadt C, Garcia-Echeverria C, van Dongen GA, Lub-de Hooge MN, Schröder CP, de Vries EG. ^{89}Zr-bevacizumab PET of early antiangiogenic tumor response to treatment with HSP90 inhibitor NVP-AUY922. J. Nucl. Med. 2010; 51:761–767. [PubMed: 20395337]

[86]. Rizvi SN, Visser OJ, Vosjan MJ, van Lingen A, Hoekstra OS, Zijlstra JM, Huijgens PC, van Dongen GA, Lubberink M. Biodistribution, radiation dosimetry and scouting of ^{90}Y-ibritumomab tiuxetan therapy in patients with relapsed B-cell non-Hodgkin's lymphoma using ^{89}Zr-ibritumomab tiuxetan and PET. Eur. J. Nucl. Med. Mol. Imaging. 2012; 39:512–520. [PubMed: 22218876]

[87]. Oude Munnink TH, Arjaans ME, Timmer-Bosscha H, Schröder CP, Hesselink JW, Vedelaar SR, Walenkamp AM, Reiss M, Gregory RC, Lub-de Hooge MN, de Vries EG. PET with the ^{89}Zr-labeled transforming growth factor-β antibody fresolimumab in tumor models. J. Nucl. Med. 2011; 52:2001–2008. [PubMed: 22072706]

[88]. Hong H, Severin GW, Yang Y, Engle JW, Zhang Y, Barnhart TE, Liu G, Leigh BR, Nickles RJ, Cai W. Positron emission tomography imaging of CD105 expression with ^{89}Zr-Df-TRC105. Eur. J. Nucl. Med. Mol. Imaging. 2012; 39:138–148. [PubMed: 21909753]

[89]. Ruggiero A, Holland JP, Hudolin T, Shenker L, Koulova A, Bander NH, Lewis JS, Grimm J. Targeting the internal epitope of prostate-specific membrane antigen with ^{89}Zr-7E11 immuno-PET. J. Nucl. Med. 2011; 52:1608–1615. [PubMed: 21908391]

[90]. Börjesson PK, Jauw YW, de Bree R, Roos JC, Castelijns JA, Leemans CR, van Dongen GA, Boellaard R. Radiation dosimetry of ^{89}Zr-labeled chimeric monoclonal antibody U36 as used for immuno-PET in head and neck cancer patients. J. Nucl. Med. 2009; 50:1828–1836. [PubMed: 19837762]

[91]. Divgi CR, Pandit-Taskar N, Jungbluth AA, Reuter VE, Gönen M, Ruan S, Pierre C, Nagel A, Pryma DA, Humm J, Larson SM, Old LJ, Russo P. Preoperative characterisation of clear-cell

renal carcinoma using iodine-124-labelled antibody chimeric G250 (124I-cG250) and PET in patients with renal masses: a phase I trial. Lancet Oncol. 2007; 8:304–310. [PubMed: 17395103]

[92]. Chacko AM, Divgi CR. Radiopharmaceutical chemistry with iodine-124: a non-standard radiohalogen for positron emission tomography. Med. Chem. 2011; 7:395–412. [PubMed: 21711220]

[93]. Sharkey RM, Karacay H, McBride WJ, Rossi EA, Chang CH, Goldenberg DM. Bispecific antibody pretargeting of radionuclides for immuno single-photon emission computed tomography and immuno positron emission tomography molecular imaging: an update. Clin. Cancer Res. 2007; 13:5577s–5585s. [PubMed: 17875792]

[94]. Koehler L, Gagnon K, McQuarrie S, Wuest F. Iodine-124: a promising positron emitter for organic PET chemistry. Molecules. 2010; 15:2686–2718. [PubMed: 20428073]

[95]. Herzog H, Tellmann L, Scholten B, Coenen HH, Qaim SM. PET imaging problems with the non-standard positron emitters Yttrium-86 and Iodine-124. Q. J. Nucl. Med. Mol. Imaging. 2008; 52:159–165. [PubMed: 18043538]

[96]. O'Donoghue JA, Smith-Jones PM, Humm JL, Ruan S, Pryma DA, Jungbluth AA, Divgi CR, Carrasquillo JA, Pandit-Taskar N, Fong Y, Strong VE, Kemeny NE, Old LJ, Larson SM. ^{124}I-huA33 antibody uptake is driven by A33 antigen concentration in tissues from colorectal cancer patients imaged by immuno-PET. J. Nucl. Med. 2011; 52:1878–1885. [PubMed: 22068895]

[97]. Carrasquillo JA, Pandit-Taskar N, O'Donoghue JA, Humm JL, Zanzonico P, Smith-Jones PM, Divgi CR, Pryma DA, Ruan S, Kemeny NE, Fong Y, Wong D, Jaggi JS, Scheinberg DA, Gonen M, Panageas KS, Ritter G, Jungbluth AA, Old LJ, Larson SM. ^{124}I-huA33 antibody PET of colorectal cancer. J. Nucl. Med. 2011; 52:1173–1180. [PubMed: 21764796]

[98]. Belov VV, Bonab AA, Fischman AJ, Heartlein M, Calias P, Papisov MI. Iodine-124 as a label for pharmacological PET imaging. Mol. Pharm. 2011; 8:736–747. [PubMed: 21361362]

[99]. Pryma DA, O'Donoghue JA, Humm JL, Jungbluth AA, Old LJ, Larson SM, Divgi CR. Correlation of *in vivo* and *in vitro* measures of carbonic anhydrase IX antigen expression in renal masses using antibody ^{124}I-cG250. J. Nucl. Med. 2011; 52:535–540. [PubMed: 21421715]

[100]. Schwartz J, Humm JL, Divgi CR, Larson SM, O'Donoghue JA. Bone marrow dosimetry using ^{124}I-PET. J. Nucl. Med. 2012; 53:615–621. [PubMed: 22414633]

[101]. Girgis MD, Olafsen T, Kenanova V, McCabe KE, Wu AM, Tomlinson JS. CA19-9 as a potential target for radiolabeled antibody-based positron emission tomography of pancreas cancer. Int. J. Mol. Imaging. 2011; 2011:834515. [PubMed: 21912743]

[102]. Zou P, Povoski SP, Hall NC, Carlton MM, Hinkle GH, Xu RX, Mojzisik CM, Johnson MA, Knopp MV, Martin EW Jr, Sun D. ^{124}I-HuCC49deltaCH2 for TAG-72 antigen-directed positron emission tomography (PET) imaging of LS174T colon adenocarcinoma tumor implants in xenograft mice: preliminary results. World J. Surg. Oncol. 2010; 6:65. [PubMed: 20691066]

[103]. Povoski SP, Hall NC, Murrey DA Jr, Sharp DS, Hitchcock CL, Mojzisik CM, Bahnson EE, Knopp MV, Martin EW Jr, Bahnson RR. Multimodal imaging and detection strategy with ^{124}I-labeled chimeric monoclonal antibody cG250 for accurate localization and confirmation of extent of disease during laparoscopic and open surgical resection of clear cell renal cell carcinoma. Surg. Innov. 2012 Epub ahead of print.

[104]. Scott AM, Lee FT, Jones R, Hopkins W, MacGregor D, Cebon JS, Hannah A, Chong G, Papenfuss PU,A, Rigopoulos A, Sturrock S, Murphy R, Wirth V, Murone C, Smyth FE, Knight S, Welt S, Ritter G, Richards E, Nice EC, Burgess AW, Old LJ. A phase I trial of humanized monoclonal antibody A33 in patients with colorectal carcinoma: biodistribution, pharmacokinetics, and quantitative tumor uptake, Clin. Cancer Res. 2005; 11:4810–4817.

[105]. Reddy S, Robinson MK. Immuno-PET in cancer models. Semin. Nucl. Med. 2010; 40:182–189. [PubMed: 20350627]

[106]. Stein R, Goldenberg DM, Thorpe SR, Basu A, Mattes MJ. Effects of radiolabeling monoclonal antibodies with a residualizing iodine radiolabel on the accretion of radioisotope in tumors. Cancer Res. 1995; 55:3132–3139. [PubMed: 7606734]

[107]. van Schaijk FG, Broekema M, Oosterwijk E, van Eerd JE, McBride BJ, Goldenberg DM, Corstens FH, Boerman OC. Residualizing iodine markedly improved tumor targeting using bispecific antibody-based pretargeting. J. Nucl. Med. 2005; 46:1016–1022. [PubMed: 15937314]

[108]. Wilbur DS, Hadley SW, Hylarides MD, Abrams PG, Beaumier PA, Morgan AC, Reno JM, Fritzberg AR. Development of a stable radioiodinating reagent to label monoclonal antibodies for radiotherapy of cancer. J. Nucl. Med. 1989; 30:216–226. [PubMed: 2738650]

[109]. U.S. Food and Drug Administration. [Accessed on: August 15, 2012] Guidance: PET Drugs-Current Good Manufacturing Practice (CGMP) (Small Entity Compliance Guide). Available at: http://www.fda.gov/downloads/drugs/GuidanceComplianceRegulatoryInformation/Guidances/ucm266640.pdf.

[110]. Zalcberg JR, Thompson CH, Lichtenstein M, Andrews J, McKenzie IF. Localization of human colorectal tumor xenografts in the nude mouse with the use of radiolabeled monoclonal antibody. J. Natl. Cancer Inst. 1983; 71:801–808. [PubMed: 6578372]

[111]. Goldenberg DM, Chang CH, Rossi EA, McBride WJ, Sharkey RM. Pretargeted molecular imaging and radioimmunotherapy. Theranostics. 2012; 2:523–540. [PubMed: 22737190]

[112]. Schoffelen R, Sharkey RM, Goldenberg DM, Franssen G, McBride WJ, Rossi EA, Chang CH, Laverman P, Disselhorst JA, Eek A, van der Graaf WT, Oyen WJ, Boerman OC. Pretargeted immuno-positron emission tomography imaging of carcinoembryonic antigen-expressing tumors with a bispecific antibody and a ^{68}Ga- and ^{18}F-labeled hapten peptide in mice with human tumor xenografts. Mol. Cancer Ther. 2010; 9:1019–1027. [PubMed: 20354120]

[113]. Aarts F, Boerman OC, Sharkey RM, Hendriks T, Chang CH, McBride WJ, Bleichrodt RP, Oyen WJ, Goldenberg DM. Pretargeted radioimmunoscintigraphy in patients with primary colorectal cancer using a bispecific anticarcinoembryonic antigen CEA X anti-didiethylenetriaminepentaacetic acid F(ab')2 antibody. Cancer. 2010; 116:1111–1117. [PubMed: 20127959]

[114]. Kenanova V, Olafsen T, Crow DM, Sundaresan G, Subbarayan M, Carter NH, Ikle DN, Yazaki PJ, Chatziioannou AF, Gambhir SS, Williams LE, Shively JE, Colcher D, Raubitschek AA, Wu AM. Tailoring the pharmacokinetics and positron emission tomography imaging properties of anti-carcinoembryonic antigen single-chain Fv-Fc antibody fragments. Cancer Res. 2005; 65:622–631. [PubMed: 15695407]

[115]. Hackel BJ, Kimura RH, Gambhir SS. Use of ^{64}Cu-labeled fibronectin domain with EGFR-overexpressing tumor xenograft: molecular imaging. Radiology. 2012; 263:179–188. [PubMed: 22344401]

[116]. Orlova A, Wållberg H, Stone-Elander S, Tolmachev V. On the selection of a tracer for PET imaging of HER2-expressing tumors: direct comparison of a ^{124}I-labeled affibody molecule and trastuzumab in a murine xenograft model. J. Nucl. Med. 2009; 50:417–425. [PubMed: 19223403]

[117]. Li L, Crow D, Turatti F, Bading JR, Anderson AL, Poku E, Yazaki PJ, Carmichael J, Leong D, Wheatcroft D, Raubitschek AA, Hudson PJ, Colcher D, Shively JE. Site-specific conjugation of monodispersed DOTA-PEGn to a thiolated diabody reveals the effect of increasing PEG size on kidney clearance and tumor uptake with improved 64-copper PET imaging. Bioconjug. Chem. 2011; 22:709–716. [PubMed: 21395337]

[118]. Viti F, Tarli L, Giovannoni L, Zardi L, Neri D. Increased binding affinity and valence of recombinant antibody fragments lead to improved targeting of tumoral angiogenesis. Cancer Res. 1999; 59:347–352. [PubMed: 9927045]

[119]. Rossin R, Kohno T, Hagooly A, Sharp T, Gliniak B, Arroll T, Chen Q, Hewig A, Kaplan-Lefko P, Friberg G, Radinsky R, Evelhoch JL, Welch MJ, Hwang DR. Characterization of ^{64}Cu-DOTA-conatumumab: a PET tracer for *in vivo* imaging of death receptor 5. J. Nucl. Med. 2011; 52:942–949. [PubMed: 21571804]

[120]. Fehm T, Müller V, Alix-Panabières C, Pantel K. Micrometastatic spread in breast cancer: detection, molecular characterization and clinical relevance. Breast Cancer Res. 2008; 10:S1. [PubMed: 19091005]

[121]. Yu JQ, Cristofanilli M. Circulating tumor cells and PET. J. Nucl. Med. 2011; 52:1501–1504. [PubMed: 21911596]

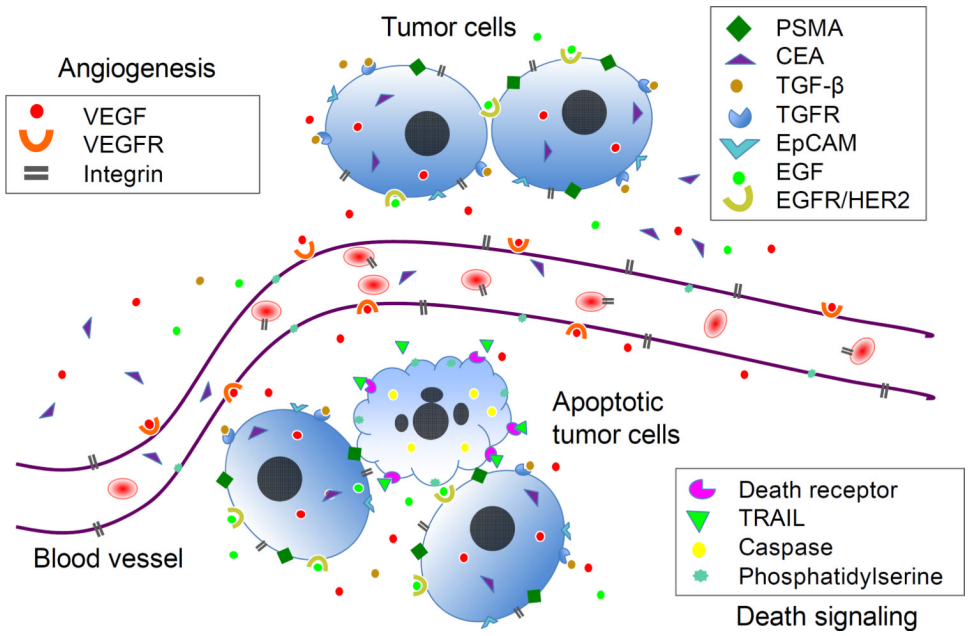

Fig. 1.

Schematic representation of potential cancer biomarkers for immuno-PET imaging. Cancer biomarkers play important roles in cancer cell proliferation, survival, angiogenesis, invasion and metastasis. The biomarkers can be associated with tumor cells (cytoplasm or surface), in the extracellular matrix (ECM) of tumor tissue, or on tumor vasculature (angiogenesis). Growth factor VEGF can be produced by tumor cells, secreted to ECM, and then bind to its receptors on endothelial cells leading to the initiation of angiogenesis. When PET imaging is employed in monitoring therapeutic efficacy, the biomarkers for cell apoptosis and necrosis, e.g. death receptors or caspase signaling can be targeted in addition to other tumor-specific targets. Note: this is for illustration purposes and does not imply that all biomarkers are present in one tumor tissue. PSMA: prostate-specific membrane antigen; CEA: carcinoembryonic antigen; TGF-β: transforming growth factor beta; TGFR: transforming growth factor receptor; EpCAM: epithelial cell adhesion molecule; EGF: epidermal growth factor; EGFR/HER-2: epidermal growth factor receptor; VEGF: vascular endothelial growth factor; VEGFR: vascular endothelial growth factor receptor; TRAIL: TNF-related apoptosis-inducing ligand.

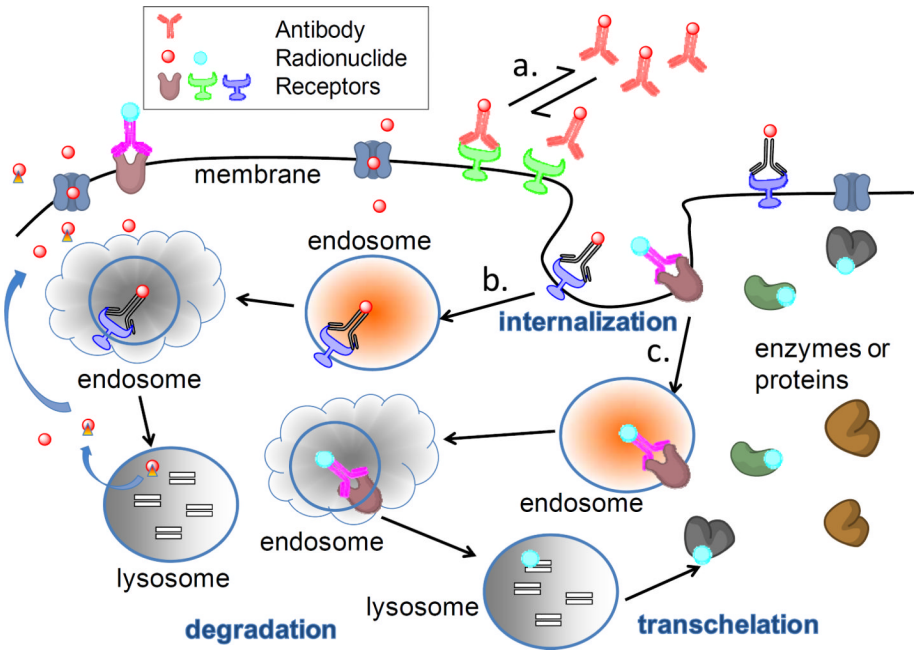

Fig. 2.

Schematic representation of the fate of antibodies (internalized or non-internalized) labeled with residualizing or non-residualizing radionuclides. **a.** a non-internalized antibody labeled with a non-residualizing radionuclide. Antibodies bind to their antigens in a dynamic association–dissociation equilibrium fashion. **b.** an internalized antibody labeled with a nonresidualizing radionuclide. After internalization and degradation of the antibody conjugates and receptors, non-residualizing radionuclides (such as ^{124}I, ^{76}Br) are released from the cell and enter the extracellular space. **c.** an internalized antibody linked with a residualizing radionuclide. After internalization and degradation of the antibody conjugates and receptors, residualizing radionuclides (such as ^{64}Cu, ^{86}Y, ^{89}Zr) can be trapped in the lysosome. Even if released from lysosome, it can transchelate to intracellular proteins and remain in the cell.

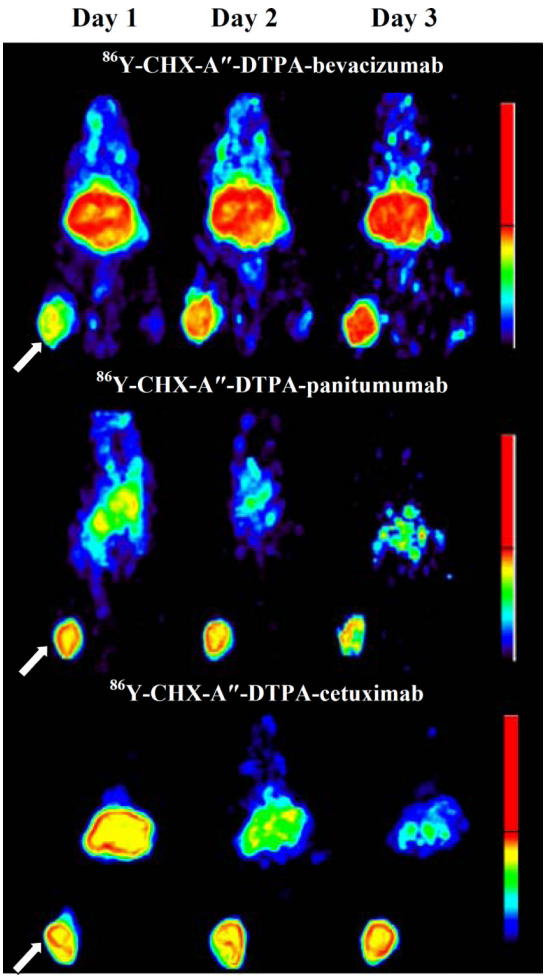

Fig. 3.

Representative immuno-PET images from day 1 to day 3 after administration of ^{86}YCHX-A”-DTPA-bevacizumab, ^{86}Y-CHX-A”-DTPA-panitumumab, ^{86}Y-CHX-A”-DTPA-cetuximab in female athymic (NCr) *nu/nu* mouse bearing VEGF-A positive human ovarian carcinoma SKOV3 xenograft (top) or human colorectal carcinoma LS-174T xenografts (middle, bottom). The tumors are indicated with a white arrow. The scale represents % maximum and minimum threshold intensity. This figure is adapted from Nayak, et al. [71,74,75].

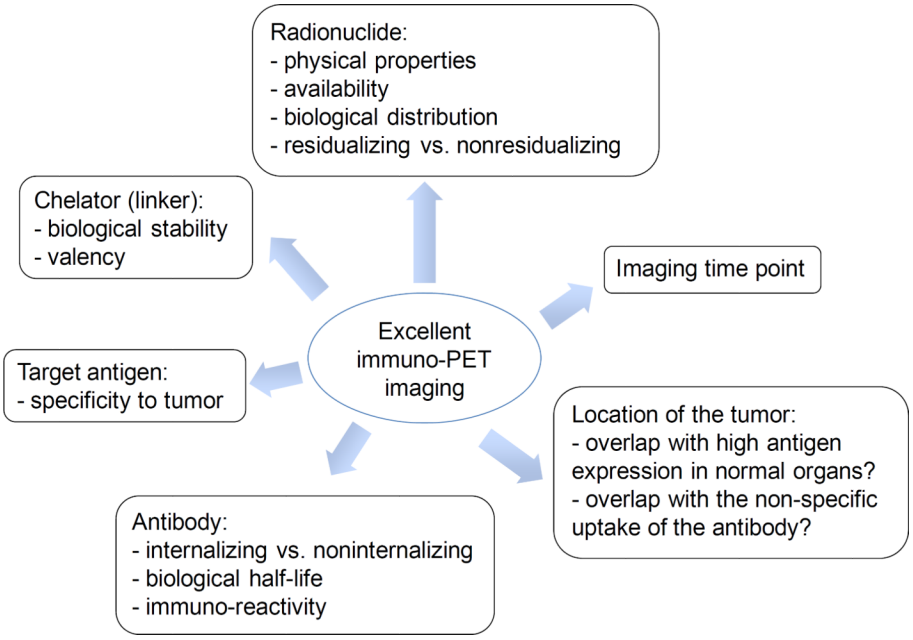

Fig. 4.
Factors to be considered when selecting a β^+ emitter.

Table 1

Criteria for an ideally effective clinical immuno-PET probe.

Number	Criteria
1	The physical half-life of the radionuclide needs to be compatible with the biological half-life of the linked antibody;
2	The target antigen should be significantly overexpressed in tumor tissues versus normal tissues;
3	The radiotracer targets tumor sensitively and specifically;
4	Rapid systemic clearance relative to the radionuclide half-life is critical to achieve high contrast imaging versus normal tissues;
5	Non-specific binding is minimal;
6	The radiotracer should be stable, so that unsafe radiometabolites are minimal and that the radionuclide remains sequestered relative to the effective half-life of the radiotracer;
7	Toxicity is low;
8	Preparation is simple and amenable to clinical radiopharmacies;
9	The radionuclide is readily available;
10	The radionuclide should have low positron energy and high positron (β^+)-decay branch ratio or abundance;
11	Cost is low.

Table 2

Characteristics of selected longer-lived β^+-emitting radionuclides for radioimmunoimaging.

Radionuclide	Half-life	Recommended timeframe	Availability	RIT radioisotope counterpart	Residualizing?	Possible accumulation sites[a]	Current application[b]	Human studies[c]	References
^{52}Mn	134.2 h	1–2 weeks	Cyclotron or reactor	N/A	Residualizing	Brain, liver, kidney, pancreas	N/A	No	16 – 20
^{55}Co	17.5 h	~ 48 hours	Cyclotron	N/A	Residualizing	Liver, kidney, bone	Brain ischemia and infarction	Yes	21 – 27
^{64}Cu	12.7 h	~ 48 hours	Cyclotron or reactor, commercially available	^{67}Cu	Residualizing	Liver, blood, spleen, lung, kidney	Cancer radiodiagnosis, RIT planning, treatment planning and monitoring	Yes (immuno -PET)	28 – 44
^{66}Ga	9.4 h	~ 36 hours	Cyclotron	^{66}Ga	Residualizing	Bone, liver, kidney, intestine	Radiodiagnosis, RIT planning	Yes	45 – 50
^{72}As	25.9 h	~ 72 hours	Cyclotron	^{77}As	Residualizing	Bone, blood cells	N/A	Yes[d]	51 – 55
^{76}Br	16.2 h	~ 48 hours	Cyclotron, commercially available	^{76}Br, ^{131}I	Non-residualizing	Blood	Radiodiagnosis, RIT planning, brain edema	Yes	56 – 70
^{86}Y	14.7 h	~ 48 hours	Cyclotron or heavy-ion accelerator, limited commercial supply[e]	^{90}Y, ^{177}Lu	Residualizing	Bone, blood, liver	RIT planning and monitoring	Yes	71 – 78
^{89}Zr	78.4 h	~ 1 week	Cyclotron or reactor, limited commercial supply	^{90}Y, ^{177}Lu	Residualizing	Bone, liver, spleen, kidney	Radioimmunodiagnosis, RIT planning, treatment planning and monitoring	Yes (immuno -PET)	79 – 90
^{124}I	100.2 h	~ 1 week	Cyclotron, commercially available	^{131}I, ^{186}Re, ^{188}Re	Non-residualizing	Thyroid gland	Pharmacodynamics, Preoperative identification, dosimetry	Yes (immuno -PET)	91 – 108

[a] *Possible accumulation sites* refer to the preferable sites for free isotopes.

[b] *Current application* refers to current studies in both animals and humans.

[c] *Human studies* include all the radionuclide-involved clinical studies not limited to radiolabeled antibodies.

[d] ^{72}As was used in humans to study environmental toxicity associated with high doses of natural arsenic [9].

[e] *Limited commercial supply* indicates that the radioisotope is limited to a small number of production sites (<5).

Table 3

Characteristics of engineered proteins.

Engineered protein	Size (kDa)	Blood clearance ($T_{1/2\beta}$)	Major route of clearance	Valency
affibody	10	5–60 min	Kidney	flexible
nanobody	15	10 min-1.5 h	Kidney	flexible
single-chain variable fragment (scFv)	25	0.5–2 h	Kidney	monovalent
diabody (scFv dimers)	50	3–7 h	Kidney	bivalent
minibody (V_L-V_H-CH_3)	80	6–11 h	Liver	bivalent
scFv-Fc	105	8 h-12 d	Liver	bivalent